CrossMark

J. Fluid Mech. (2016), *vol.* 788, *pp.* 767–796. © Cambridge University Press 2016
doi:10.1017/jfm.2015.718

Shear flow instabilities in shallow-water magnetohydrodynamics

J. Mak[1,†], S. D. Griffiths[1] and D. W. Hughes[1]

[1]Department of Applied Mathematics, University of Leeds, Leeds LS2 9JT, UK

(Received 31 January 2015; revised 9 October 2015; accepted 2 December 2015;
first published online 14 January 2016)

Within the framework of shallow-water magnetohydrodynamics, we investigate the linear instability of horizontal shear flows, influenced by an aligned magnetic field and stratification. Various classical instability results, such as Høiland's growth-rate bound and Howard's semi-circle theorem, are extended to this shallow-water system for quite general flow and field profiles. In the limit of long-wavelength disturbances, a generalisation of the asymptotic analysis of Drazin & Howard (*J. Fluid Mech.*, vol. 14, 1962, pp. 257–283) is performed, establishing that flows can be distinguished as either shear layers or jets. These possess contrasting instabilities, which are shown to be analogous to those of certain piecewise-constant velocity profiles (the vortex sheet and the rectangular jet). In both cases it is found that the magnetic field and stratification (as measured by the Froude number) are generally each stabilising, but weak instabilities can be found at arbitrarily large Froude number. With this distinction between shear layers and jets in mind, the results are extended numerically to finite wavenumber for two particular flows: the hyperbolic-tangent shear layer and the Bickley jet. For the shear layer, the instability mechanism is interpreted in terms of counter-propagating Rossby waves, thereby allowing an explication of the stabilising effects of the magnetic field and stratification. For the jet, the competition between even and odd modes is discussed, together with the existence at large Froude number of multiple modes of instability.

Key words: instability, magnetohydrodynamics, shallow water flows

1. Introduction

The interaction of horizontal shear flows and magnetic fields in stably stratified layers is central to many problems in astrophysical fluid dynamics – involving, for example, planetary interiors, stellar radiative zones and accretion discs. An important example of such a flow, which has received considerable attention recently, is that of the solar tachocline (see Hughes, Rosner & Weiss 2007). The tachocline, discovered via helioseismic observations, is a thin layer in the Sun, extending downwards from the (neutrally stable) base of the convective zone to the (stably stratified) top of the radiative interior, characterised by radial velocity shear and also planetary-scale

† Present address: School of Mathematics and Maxwell Institute for Mathematical Sciences, University of Edinburgh, Edinburgh EH9 3FD, UK. Email address for correspondence: julian.c.l.mak@googlemail.com

https://doi.org/10.1017/jfm.2015.718 Published online by Cambridge University Press

horizontal shears associated with the equator to pole differential rotation of the Sun. Most models of the solar dynamo invoke the tachocline as the site for the storage and generation of the Sun's strong, predominantly toroidal, magnetic field.

Here we are interested in the stability of stably stratified flows with horizontal shear and an aligned field in a quite general context. It is possible to examine the stability of such flows in a continuously stratified three-dimensional setting (e.g. Miura & Pritchett 1982; Cally 2003). However, we adopt the alternative approach of considering the dynamics of a thin fluid layer under the shallow-water approximation, which is valid when the horizontal length scale of the motion is long compared with the depth of the fluid layer, as is typically the case in large-scale astrophysical flows. This leads to a set of two-dimensional partial differential equations, with no explicit dependence on the vertical coordinate, which offers a considerable mathematical simplification. Such shallow-water equations capture the fundamental dynamics of density stratification, including gravity waves, and allow the interaction of stratification with horizontal shear flows and magnetic fields to be analysed in the simplest possible setting.

Hydrodynamic shallow-water models, which date back to Laplace, are derived by considering a thin fluid layer of constant density bounded below by a rigid medium and above by a fluid of negligible inertia (e.g. Vallis 2006, § 3.1). The corresponding reduction for electrically conducting fluids – the shallow-water magnetohydrodynamic (SWMHD) equations of Gilman (2000) – additionally requires the fluid layer to be a perfect conductor, and to be bounded above and below by perfect conductors. There are few direct astrophysical analogues for such a configuration. However, we can borrow an important idea from planetary atmospheric dynamics, where the hydrodynamic shallow-water equations are widely used to understand waves and instabilities in a continuously stratified atmospheric layer. This is justified because there is a formal mathematical analogy between the linearised equations in the two systems, provided the layer depth in the shallow-water model is taken to be a so-called equivalent depth (e.g. Gill 1982, § 6.11), so that the shallow-water gravity wave speed (in the horizontal) matches that of (the fastest) gravity waves in a continuously stratified layer. We have this analogy in mind throughout this study.

The SWMHD equations have been widely studied in recent years. They have been shown to possess a hyperbolic as well as a Hamiltonian structure (De Sterck 2001; Dellar 2002), and to support wave motions such as inertia–gravity waves and Alfvén waves (Schecter, Boyd & Gilman 2001; Zaqarashvili *et al.* 2007; Heng & Spitkovsky 2009). As reviewed by Gilman & Cally (2007), they have also been used to study the linear instability of shear flows in the tachocline; these studies considered basic states that were functions only of latitude, investigating the dependence of the instabilities on the strength and spatial structure of the magnetic field and on a (reduced) gravity parameter (Gilman & Dikpati 2002; Dikpati, Gilman & Rempel 2003).

Here we investigate the simplest general model of shear flow instabilities in SWMHD. Specifically, we consider the linear instability of a steady parallel flow and aligned magnetic field, both sheared in the horizontal cross-stream direction, in the inviscid and perfectly electrically conducting limit. We use a planar geometry, which is immediately applicable to local shear zones, and which could also apply to planetary-scale shears with appropriate care. In this first study, we consider the case with no background rotation, which will be the best model for certain astrophysical objects. Even if background rotation is dynamically important, it is nonetheless crucial to understand the non-rotating problem before rotation is added. We are thus left to investigate how the prototypical flows are modified by the combined action of magnetic fields and stratification, which, in isolation, are generally thought to

https://doi.org/10.1017/jfm.2015.718 Published online by Cambridge University Press

be stabilising. The limits with no field (i.e. hydrodynamic shallow water) or no stratification (i.e. incompressible two-dimensional MHD) are both well studied, as is the classical case with neither magnetic field nor stratification. We are thus able to draw upon ideas and methods from a substantial literature (e.g. Drazin & Howard 1966; Drazin & Reid 1981; Vallis 2006).

We start, in § 2, by formulating the linear instability problem for plane-parallel basic states with the flow and field dependent on the cross-stream direction. In § 3 we derive extensions of classical growth-rate bounds, semi-circle theorems, stability criteria and parity results for modal solutions for quite general basic states. In § 4 we develop the fundamental idea that background flows belong to one of two distinct classes – shear flows and jets – possessing contrasting instabilities. This classification is first investigated analytically for the simplest shear flow (the vortex sheet, § 4.1) and the simplest jet (the rectangular jet, § 4.2). The justification for this is that analogous behaviour can be found for smooth profiles with long-wavelength disturbances; this is demonstrated in § 4.3 by extending the analysis of Drazin & Howard (1962) to SWMHD. Together, these results introduce certain key ideas: the existence of wavenumber cutoffs, a tendency for stabilisation by field or stratification, and the possibility of destabilisation by field and stratification acting together. We then show that these characteristics also hold for less idealised cases, i.e. smooth flows with finite wavenumber disturbances. This is demonstrated numerically for a shear flow (the hyperbolic tanh profile, § 5.1) and a jet (the Bickley jet, § 5.2), with a discussion of the instability mechanisms where possible. Possible applications to the solar tachocline and future extensions of the work are discussed in § 6.

2. Mathematical formulation

2.1. *Governing equations*

We consider a thin layer of perfectly electrically conducting fluid moving under the influence of gravity. We use a Cartesian geometry, with horizontal coordinates x and y, and an upwards pointing coordinate z. At time t, the fluid, which is taken to be inviscid and of constant density ρ, has a free surface at $z = h(x, y, t)$ and is bounded below by a rigid impermeable boundary at $z = -H(x, y)$.

We consider motions with a characteristic horizontal length scale L_0 that is long compared with a characteristic layer depth H_0. One can then make a shallow-water reduction in which the vertical momentum balance is taken to be magnetohydrostatic, and for which the horizontal velocity $\boldsymbol{u}$ and horizontal magnetic field $\boldsymbol{B}$ are independent of z. When the bottom boundary is perfectly electrically conducting (and is thus a magnetic field line) and the free surface remains a field line, the magnetic shallow-water equations of Gilman (2000) are obtained. These are an extension of the classical shallow-water equations of geophysical fluid dynamics.

We use these equations in non-dimensional form. We denote the characteristic horizontal velocity of the basic state by U_0, and the characteristic magnetic field strength by B_0. Non-dimensionalising x and y by L_0, t by the advective time scale L_0/U_0, H by H_0, h by U_0^2/g (where g is the acceleration due to gravity), velocity by U_0 and magnetic field by B_0, the SWMHD equations are

$$\frac{\partial \boldsymbol{u}}{\partial t} + \boldsymbol{u}\cdot\nabla\boldsymbol{u} = -\nabla h + M^2\boldsymbol{B}\cdot\nabla\boldsymbol{B}, \tag{2.1a}$$

$$\frac{\partial \boldsymbol{B}}{\partial t} + \boldsymbol{u}\cdot\nabla\boldsymbol{B} = \boldsymbol{B}\cdot\nabla\boldsymbol{u}, \tag{2.1b}$$

$$F^2\frac{\partial h}{\partial t} + \nabla\cdot((H + F^2 h)\boldsymbol{u}) = 0, \tag{2.1c}$$

https://doi.org/10.1017/jfm.2015.718 Published online by Cambridge University Press

where $F = U_0/\sqrt{gH_0}$ and $M = (B_0/\sqrt{\mu\rho})/U_0$, with μ being the permeability of the fluid. In addition to (2.1*a–c*), the shallow-water reduction implies

$$\boldsymbol{\nabla}\cdot((H+F^2h)\boldsymbol{B}) = 0. \tag{2.2}$$

However, (2.2) need not be considered explicitly, since, if it is satisfied at some initial time, then (2.1*a–c*) guarantee that it remains satisfied for all time.

The system has two non-dimensional parameters. The Froude number F is the ratio of the characteristic horizontal velocity of the basic state to the gravity wave speed $\sqrt{gH_0}$ (and is related to the reduced gravity parameter G of Gilman & Dikpati (2002) via $G = F^{-2}$). The parameter M is the ratio of the Alfvén wave speed $B_0/\sqrt{\mu\rho}$ to the characteristic horizontal velocity of the basic state. When H is constant and $F \to 0$, (2.1*c*) and (2.2) become $\boldsymbol{\nabla}\cdot\boldsymbol{u} = 0$ and $\boldsymbol{\nabla}\cdot\boldsymbol{B} = 0$, respectively, and we recover the equations for two-dimensional incompressible magnetohydrodynamics, with h playing the role of pressure. When $M \to 0$, (2.1*b*) decouples from (2.1*a*) and (2.1*c*), and we recover the hydrodynamic shallow-water equations; these have a well-known correspondence with two-dimensional compressible hydrodynamics (e.g. Vallis 2006, § 3.1), which we exploit from time to time.

As an example of astrophysical parameter values, we estimate M and F in the solar tachocline, using data from Gough (2007). We set U_0 to be the equator-to-pole difference in the zonal velocity, implying $U_0 \approx 200$ m s^{-1}. This is appropriate for planetary-scale disturbances; for local shear zones, one might take $U_0 \approx 20$ m s^{-1}. There is considerable uncertainty in the strength of the magnetic field in the tachocline (Hughes *et al.* 2007), although a likely range is 10^3 G $\lesssim B_0 \lesssim 10^5$ G. Then, taking $\rho = 210$ kg m^{-3}, we find $0.03 \lesssim M \lesssim 3$. To estimate F, we must choose a gravity wave speed $\sqrt{gH_0}$ for the layer. One means of doing this is to take H_0 to be the depth of the tachocline and to interpret g as a reduced gravity, accounting for the fractional density difference of the overlying fluid, as in Dikpati & Gilman (2001). The reduced gravity may also be constructed by considering a thin active layer between two deeper passive layers (cf. Vallis 2006, § 3.2). However, here we pursue the analogy between shallow-water flows and those of a continuously stratified layer with buoyancy frequency N and depth H_1, and choose $\sqrt{gH_0}$ to be the speed of the fastest gravity wave in such a layer, which is NH_1/π (Gill 1982, § 6.11). Taking $H_1 \approx 2 \times 10^7$ m (i.e. $0.03R_\odot$, where $R_\odot$ is the solar radius) and $N \approx 8 \times 10^{-4}$ s^{-1}, which are bulk values that might describe a mode spanning the entire tachocline, gives a gravity wave speed $NH_1/\pi = \sqrt{gH_0} \approx 5000$ m s^{-1}, corresponding to an equivalent depth $H_0 \approx 50$ km (taking $g \approx 540$ m s^{-2}). Again taking $U_0 \approx 200$ m s^{-1}, we thus estimate $F \approx 0.04$, although it is clear that F would be somewhat smaller or larger if one considered motions towards the top of the radiative zone (with stronger stratification) or towards the base of the convection zone (with weaker stratification).

2.2. *The linear instability problem*

Above a topography of the form $H = H(y)$, we consider a basic state $h = 0$, $\boldsymbol{u} = U(y)\boldsymbol{e}_x$ and $\boldsymbol{B} = B(y)\boldsymbol{e}_x$, so that the magnetic field is initially aligned with the flow. We then consider the linear evolution of perturbations in h, $\boldsymbol{u} = (u, v)$ and $\boldsymbol{B} = (b_x, b_y)$, governed by

https://doi.org/10.1017/jfm.2015.718 Published online by Cambridge University Press

$$\left(\frac{\partial}{\partial t}+U\frac{\partial}{\partial x}\right)u+U'v=-\frac{\partial h}{\partial x}+M^2\left(B\frac{\partial b_x}{\partial x}+B'b_y\right), \tag{2.3a}$$

$$\left(\frac{\partial}{\partial t}+U\frac{\partial}{\partial x}\right)v=-\frac{\partial h}{\partial y}+M^2B\frac{\partial b_y}{\partial x}, \tag{2.3b}$$

$$\left(\frac{\partial}{\partial t}+U\frac{\partial}{\partial x}\right)b_x+B'v=B\frac{\partial u}{\partial x}+U'b_y, \tag{2.3c}$$

$$\left(\frac{\partial}{\partial t}+U\frac{\partial}{\partial x}\right)b_y=B\frac{\partial v}{\partial x}, \tag{2.3d}$$

$$F^2\left(\frac{\partial}{\partial t}+U\frac{\partial}{\partial x}\right)h+H\left(\frac{\partial u}{\partial x}+\frac{\partial v}{\partial y}\right)+H'v=0, \tag{2.3e}$$

where a prime denotes differentiation. The y-dependence of the basic state allows perturbations of the form

$$\xi(x,y,t)=\mathrm{Re}\{\hat{\xi}(y)\exp(\mathrm{i}\alpha(x-ct))\}, \tag{2.4}$$

where α is the (real) wavenumber and c is the (complex) phase speed. Manipulation of (2.3), and dropping hats, leads to the single equation

$$\left(\frac{S^2(Hv)'}{H(U-c)^2K^2}\right)'-\left(\frac{\alpha^2S^2}{H(U-c)^2}-\frac{U'}{H(U-c)}\left(\frac{S^2}{(U-c)^2K^2}\right)'+\frac{Q'S^2}{(U-c)^3K^2}\right)Hv=0, \tag{2.5}$$

where $Q=-U'/H$ is the background potential vorticity, and

$$S^2(y)=(U(y)-c)^2-M^2B^2(y),\quad K^2(y)=1-\frac{F^2S^2(y)}{H(y)}. \tag{2.6a,b}$$

Following Howard (1961), under the transformation $Hv=(U-c)G$, (2.5) becomes

$$\left(\frac{S^2}{K^2}\frac{G'}{H}\right)'-\frac{\alpha^2S^2}{H}G=0. \tag{2.7}$$

We shall use this more compact form for the remainder of this study. In the non-magnetic shallow-water limit ($M=0$), (2.5) reduces to equation (3.4) of Balmforth (1999). In the two-dimensional incompressible magnetohydrodynamic limit ($F=0$ and $H=1$), (2.7) reduces to equation (3.5) of Hughes & Tobias (2001).

We shall consider (2.7) in either an unbounded domain, for which $|G|\to 0$ as $|y|\to\infty$, or in a bounded domain with rigid side walls at $y=\pm L$, where $G=0$ and hence $b_y=0$ via (2.3*d*). Either way, for given real α, (2.7) is then an eigenvalue problem for the unknown phase speed $c=c_r+\mathrm{i}c_i$. We will focus on instabilities, i.e. $c_i\neq 0$, in which case (2.7) has no singularities for real values of y. Since the transformation $\alpha\to-\alpha$ leaves (2.7) unchanged, we may take $\alpha\geqslant 0$ without loss of generality. Instability then occurs if $c_i>0$, with growth rate αc_i.

3. General theorems

In this section we derive three results that hold for general shear flows $U(y)$: two provide bounds on the growth rate of any instability, whereas the third concerns implications of the parity of the basic state flow.

https://doi.org/10.1017/jfm.2015.718 Published online by Cambridge University Press

3.1. *Growth-rate bound*

A bound on the instability growth rate may be obtained by calculating the rate of change of the total disturbance energy using the combination

$$Hu^* \times (2.3a) + Hv^* \times (2.3b) + (M^2 H b_x^*) \times (2.3c) + (M^2 H b_y^*) \times (2.3d) + h^* \times (2.3e), \tag{3.1}$$

where * denotes complex conjugate. On adopting the form (2.4) for the perturbations, the real part of this expression gives (on dropping hats)

$$\begin{aligned} &\alpha c_i (H(|u|^2 + |v|^2 + M^2|b_x|^2 + M^2|b_y|^2) + F^2|h|^2) \\ &\quad = -\mathrm{Re}(HU'(vu^* - M^2 b_x^* b_y) + M^2 HB'(vb_x^* - u^* b_y)) - \mathrm{Re}\left(\frac{\mathrm{d}}{\mathrm{d}y}(Hvh^*)\right). \end{aligned} \tag{3.2}$$

On integrating over the y domain, employing the boundary condition on v and manipulating the remaining terms on the right-hand side using $\pm 2\mathrm{Re}\,(pq^*) \leqslant |p|^2 + |q|^2$, we obtain the following bound on the growth rate:

$$\alpha c_i \leqslant \tfrac{1}{2}(\max|U'| + M \max|B'|). \tag{3.3}$$

In the absence of a magnetic field, this reduces to the well-known bound in hydrodynamics (Høiland 1953; Howard 1961).

3.2. *Semi-circle theorems*

In a classic paper, Howard (1961) proved that for incompressible hydrodynamic parallel shear flows, the wave speed c of any unstable mode must lie within a semi-circle in the complex plane determined by properties of the basic state flow. Subsequently, semi-circle theorems have been derived for several other hydrodynamical and hydromagnetic systems (e.g. Collings & Grimshaw 1980; Hayashi & Young 1987; Shivamoggi & Debnath 1987; Hughes & Tobias 2001). In a similar manner, a semi-circle theorem may be derived for the SWMHD system.

Multiplying (2.7) by G^*, integrating over y and using the boundary condition on v (and hence G) gives the relation

$$\int \frac{S^2}{K^2}\frac{|G'|^2}{H}\,\mathrm{d}y + \alpha^2 \int \frac{S^2|G|^2}{H}\,\mathrm{d}y = 0, \tag{3.4}$$

where S and K are functions of c given in (2.6). The imaginary part of (3.4) gives

$$c_i \int (U - c_r)\chi\,\mathrm{d}y = 0, \quad \text{where } \chi = \frac{|G'|^2}{H|K|^4} + \alpha^2\frac{|G|^2}{H} \geqslant 0. \tag{3.5}$$

Equation (3.5) immediately yields Rayleigh's result that for unstable modes (i.e. $c_i > 0$), c_r lies in the range of U (i.e. $U_{min} \leqslant c_r \leqslant U_{max}$, where the subscripts 'min' and 'max' refer to the minimum and maximum values across the domain).

On using (3.5), the real part of (3.4) gives

$$(c_r^2 + c_i^2)\int \chi\,\mathrm{d}y = \int \chi(U^2 - M^2B^2)\,\mathrm{d}y - F^2 \int \frac{|S|^4}{H|K|^4}|G'|^2\,\mathrm{d}y, \tag{3.6}$$

https://doi.org/10.1017/jfm.2015.718 Published online by Cambridge University Press

which implies that

$$0 \leqslant (c_r^2 + c_i^2) \int \chi \, \mathrm{d}y \leqslant (U^2 - M^2 B^2)_{max} \int \chi \, \mathrm{d}y. \tag{3.7}$$

This gives the first semi-circle bound: the complex wave speed c of an unstable eigenfunction must lie within the region defined by

$$c_r^2 + c_i^2 \leqslant (U^2 - M^2 B^2)_{max}. \tag{3.8}$$

The second semi-circle bound is obtained, in the standard manner, from the inequality $0 \geqslant \int (U - U_{max})(U - U_{min}) \chi \, \mathrm{d}y$. Substituting from (3.5) and deriving an inequality from (3.6) leads to the expression

$$0 \geqslant (c_r^2 + c_i^2 - (U_{min} + U_{max}) c_r + U_{min} U_{max} + M^2 (B^2)_{min}) \int \chi \, \mathrm{d}y, \tag{3.9}$$

which gives the second semi-circle bound: the speed c of an unstable eigenfunction must lie within the region defined by

$$\left(c_r - \frac{U_{min} + U_{max}}{2} \right)^2 + c_i^2 \leqslant \left(\frac{U_{max} - U_{min}}{2} \right)^2 - M^2 (B^2)_{min}. \tag{3.10}$$

Thus, taking these results together, the eigenvalue c of an unstable mode must lie within the intersection of the two semi-circles defined by (3.8) and (3.10). In the absence of a magnetic field, semi-circle (3.10) lies wholly within semi-circle (3.8), and we recover the well-known result of Howard (1961). However, as observed by Hughes & Tobias (2001), who considered the stability of aligned fields and flows in incompressible MHD, for non-zero magnetic field there is the possibility of the two semi-circles overlapping, being disjoint or indeed ceasing to exist; thus, in addition to giving eigenvalue bounds for unstable modes, these results also provide sufficient conditions for stability. From (3.8) and (3.10) it therefore follows that the basic state is linearly stable if any one of the following three conditions is satisfied:

$$M|B| \geqslant |U| \quad \text{everywhere in the domain;} \tag{3.11}$$

$$M|B|_{min} \geqslant \frac{|U_{max} - U_{min}|}{2}; \tag{3.12}$$

$$\frac{U_{max} + U_{min}}{2} - \sqrt{\left(\frac{U_{max} - U_{min}}{2} \right)^2 + M^2 (B^2)_{min}} \geqslant \sqrt{\left(U^2 - M^2 B^2 \right)_{max}}. \tag{3.13}$$

These results are equivalent to those given by Hughes & Tobias (2001) for incompressible MHD.

A drawback of the growth-rate bound (3.3) and the semi-circle bounds (3.11)–(3.13) is that they do not contain the Froude number F. Although it is possible to introduce F into the semi-circle bounds using similar manipulations to those employed by Pedlosky (1964), this does not sharpen the bound (Mak 2013), and we thus omit it.

https://doi.org/10.1017/jfm.2015.718 Published online by Cambridge University Press

3.3. *Consequences of basic state parity*

For the hydrodynamic case, it can be shown that symmetries of the basic state lead to symmetries in the stability problem (Howard 1963). These results may be generalised to SWMHD if we make the further assumptions that $B^2(y)$ and $H(y)$ are even functions about $y=0$.

We first consider the case when $U(y)$ is odd about $y=0$. Equation (2.7) is unchanged under $c\to -c$ and $G(y)\to G(-y)$. Since the equation is also unchanged under $c\to c^*$ and $G\to G^*$, it follows that an eigenfunction with eigenvalue $c=c_r+c_i$ must be accompanied by eigenfunctions with $c=\pm c_r\pm \mathrm{i}c_i$. Thus unstable solutions either have $c_r=0$ or are a pair of counter-propagating waves with the same phase speed. As argued by Howard (1963), the symmetry in the basic state implies that there is no preferred direction for wave propagation, consistent with the form of the eigenvalues.

Now consider the case when $U(y)$ is even about $y=0$. Then

$$G_e(y)=\tfrac{1}{2}(G(y)+G(-y)) \quad \text{and} \quad G_o(y)=\tfrac{1}{2}(G(y)-G(-y)) \tag{3.14a,b}$$

are also eigenfunctions of (2.7). Following Drazin & Howard (1966), if we now take G_o multiplied by (2.7) with $G=G_e$ and subtract this from G_e multiplied by (2.7) with $G=G_o$, integrating over $-L\leqslant y\leqslant L$ gives

$$W(G_e,G_o)\equiv [G_e'G_o-G_o'G_e]_{-L}^{+L}=\text{const.}=0, \tag{3.15}$$

owing to the imposed boundary conditions on the eigenfunction. The vanishing of the Wronskian W implies that the functions G_e and G_o are linearly dependent throughout the domain, which is possible only if one of them is identically zero. Thus an unstable eigenfunction corresponding to a particular eigenvalue is either an even or odd function about $y=0$.

4. Shear flows and jets: instability to long-wavelength disturbances

In classical hydrodynamic stability (i.e. $F=M=0$), there are universal scalings for the instability of an arbitrary shear flow in the long-wavelength limit $\alpha\ll 1$ (Drazin & Howard 1962, 1966). In this limit, any flow can be classified as either a shear layer (with a complex phase speed of order unity) or a jet (with a complex phase speed of order $\alpha^{1/2}$). Long-wavelength theory therefore naturally identifies two classes of flows, each with fundamentally distinct modes of instability. Here we extend this analysis to SWMHD, obtaining explicit analytical expressions for the phase speed and growth rate for both shear layers and jets, which may be used to identify various stabilisation and destabilisation effects in terms of F and M. It turns out that equivalent expressions can be obtained by considering the simpler problems of the instability of the vortex sheet and the top-hat jet. We therefore first analyse these two piecewise constant flows in §§ 4.1 and 4.2, before extending the analysis of Drazin & Howard (1962) to arbitrary smooth flows in § 4.3. Throughout this section, for simplicity, we take $H=1$ (no topography) and $B=1$ (a uniform magnetic field); we also impose

$$|G|\to 0 \quad \text{as} \quad |y|\to\infty. \tag{4.1}$$

https://doi.org/10.1017/jfm.2015.718 Published online by Cambridge University Press

4.1. *Vortex sheet*

The vortex sheet velocity profile is given by

$$U(y) = \begin{cases} +1, & y > 0, \\ -1, & y < 0. \end{cases} \tag{4.2}$$

Then, for $y \neq 0$, (2.7) becomes $G'' - \alpha^2 K^2 G = 0$. Since $U(y)$ is discontinuous at $y = 0$, the eigenfunction G must satisfy two jump conditions at $y = 0$. In the usual way, the (linearised) kinematic boundary condition implies

$$\left[\frac{v}{U-c}\right]_{0^-}^{0^+} = [G]_{0^-}^{0^+} = 0. \tag{4.3a}$$

The pressure (or free-surface displacement) is also continuous at $y = 0$. The corresponding condition on G is most easily derived by integrating (2.7) across $y = 0$, yielding

$$\left[\frac{S^2}{K^2} G'\right]_{0^-}^{0^+} = 0. \tag{4.3b}$$

Using (4.1) and (4.3*a*), we thus find

$$G(y) = \begin{cases} \exp(-\alpha K_+ y), & y > 0, \\ \exp(+\alpha K_- y), & y < 0, \end{cases} \tag{4.4}$$

where

$$K_\pm(c) = \sqrt{1 - F^2((1 \mp c)^2 - M^2)}, \quad \mathrm{Re}(K_\pm) > 0. \tag{4.5}$$

The second jump condition (4.3*b*) then implies the eigenvalue relation for c:

$$\frac{(1-c)^2 - M^2}{K_+} + \frac{(1+c)^2 - M^2}{K_-} = 0. \tag{4.6}$$

Note that c is independent of the wavenumber α, so any unstable mode with $c_i > 0$ has an unbounded growth rate as $\alpha \to \infty$. This is an artefact of considering ideal fluids; viscosity will preferentially suppress small scales and remove this unphysical behaviour.

There are several special cases. When $F = M = 0$, we recover the classical Kelvin–Helmholtz instability with $c = \pm \mathrm{i}$. When $F = 0$ but $M \neq 0$, (4.6) reduces to the incompressible MHD case of Michael (1955), with $c^2 = -(1 - M^2)$; thus, the Kelvin–Helmholtz instability is stabilised when $M \geqslant 1$, since the disturbance has to do work to bend the field lines. When $M = 0$ but $F \neq 0$, (4.6) gives the classical hydrodynamic shallow-water dispersion relation, which is analogous to that of two-dimensional compressible hydrodynamics. The Kelvin–Helmholtz instability is stabilised when $F \geqslant \sqrt{2}$ (Miles 1958; Bazdenkov & Pogutse 1983), since the disturbance has to do work to move the free surface against gravity. Thus, increasing F or M in the absence of the other is stabilising.

https://doi.org/10.1017/jfm.2015.718 Published online by Cambridge University Press

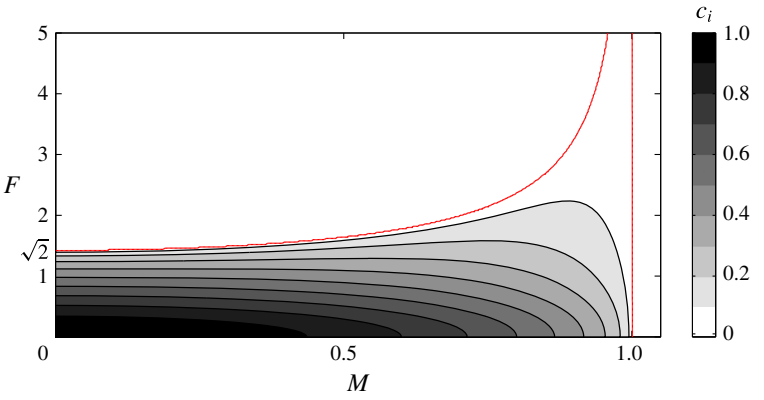


FIGURE 1. (Colour online) Contours of $\mathrm{Im}(c_v)$, given by expression (4.8), with stability boundaries (4.9*a*,*b*) in red.

In the general case where F and M are both non-zero, (4.6) can be rearranged and squared to yield a quartic equation for c:

$$F^2c^4 - 2(1+F^2(M^2+1))c^2 + (M^2-1)(2+F^2(M^2-1)) = 0. \tag{4.7}$$

Here we have ignored the degenerate case with $c = 0$, which is a solution of (4.6) when $M = 1$. By comparing solutions of (4.7) with those of (4.6) found using a Newton iteration method, we find that only two roots of (4.7) also satisfy (4.6): these are $c = \pm c_v$, where

$$c_v = \mathrm{i}\left(\frac{\sqrt{1+4F^2+4F^4M^2} - (1+F^2+F^2M^2)}{F^2}\right)^{1/2}. \tag{4.8}$$

A contour plot of $\mathrm{Im}\,(c_v)$ is shown in figure 1. From (4.8), there is instability only if

$$M < 1 \quad \text{and} \quad F < F_c = \sqrt{\frac{2}{1-M^2}}. \tag{4.9a,b}$$

Although increasing F is always stabilising at fixed M, the critical value of F above which the flow is stable increases as M increases towards 1. Thus, although magnetic field and free-surface effects are stabilising in isolation, together they can lead to instabilities at arbitrarily large values of F, provided

$$1 - \frac{2}{F^2} < M^2 < 1. \tag{4.10}$$

Using an asymptotic analysis, it is possible to investigate these instabilities further at large F and with M just smaller than unity. Rewriting (4.8) in terms of $1-M^2$ and expanding for $|1-M^2| \ll 1$, we obtain

$$c_v \sim \mathrm{i}\left(\frac{1-M^2}{1+2F^2} - \frac{2F^6(1-M^2)^2}{(1+2F^2)^3}\right)^{1/2}, \quad |1-M^2| \ll 1, \tag{4.11}$$

where terms of $O((1-M^2)^3)$ have been neglected. When $F = O(1)$, the first term on the right-hand side of (4.11) dominates. However, in the regime of interest (4.10), with

https://doi.org/10.1017/jfm.2015.718 Published online by Cambridge University Press

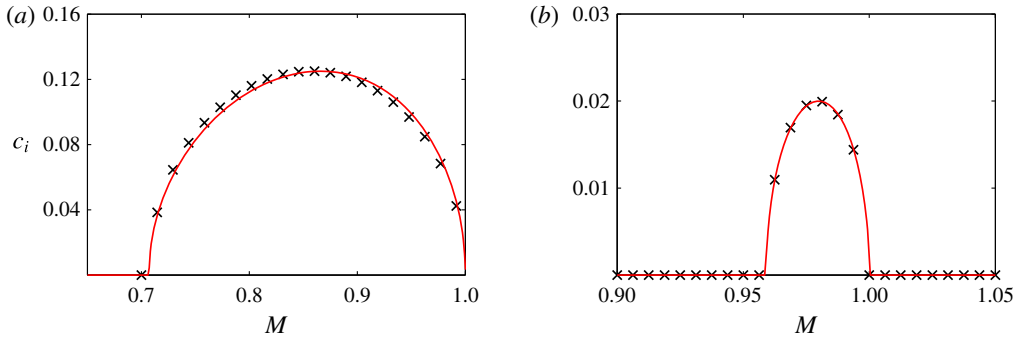


FIGURE 2. (Colour online) The weak instability regime of the vortex sheet for (*a*) $F=2$, (*b*) $F=5$, as determined directly from (4.8) (crosses) and from the asymptotic result (4.12) (line).

$F^2 \sim (1-M^2)^{-1} \gg 1$, the two terms on the right-hand side of (4.11) have the same order of magnitude, and instead we obtain

$$c_v \sim \mathrm{i}\left(\frac{1-M^2}{2F^2} - \frac{(1-M^2)^2}{4}\right)^{1/2} \quad \text{as } F^{-2} \sim (1-M^2) \to 0. \tag{4.12}$$

This simple formula is consistent with both stability boundaries in (4.9), and, as shown in figure 2, closely predicts c_i in this weak-instability regime, even when F is of order unity. Using (4.12), it is straightforward to show that $\mathrm{Im}\,(c_v)$ is maximised when $M^2 = 1 - 1/F^2$, with $c_v \sim \mathrm{i}/(2F^2)$, so that the growth rate of the most unstable mode decays like F^{-2} in this regime.

4.2. *Rectangular jet*

We now consider the top-hat velocity profile

$$U(y) = \begin{cases} 1, & |y| < 1, \\ 0, & |y| > 1. \end{cases} \tag{4.13}$$

Then (2.7) and (4.1) imply

$$G = \begin{cases} A_+ \exp(-\alpha K_0(y-1)), & y > +1, \\ A_e \cosh(\alpha K_1 y) + A_o \sinh(\alpha K_1 y), & |y| < 1, \\ A_- \exp(+\alpha K_0(y+1)), & y < -1, \end{cases} \tag{4.14}$$

for some A_+, A_-, A_e and A_o, where

$$K_0 = \sqrt{1 - F^2(c^2 - M^2)}, \quad \text{with } \mathrm{Re}(K_0) > 0 \text{ for bounded solutions}, \tag{4.15a}$$

$$K_1 = \sqrt{1 - F^2((1-c)^2 - M^2)}, \quad \text{with } -\frac{\pi}{2} < \arg(K_1) \leqslant \frac{\pi}{2}. \tag{4.15b}$$

Here we follow Rayleigh's formulation (Drazin & Reid 1981) and consider eigenfunctions that are either even or odd. For the even mode, we set $A_o = 0$,

https://doi.org/10.1017/jfm.2015.718 Published online by Cambridge University Press

$A_+ = A_-$ and write $c = c_e$. Then the jump conditions ((4.3*a*,*b*) applied at $y = \pm 1$) and (4.14) give

$$\frac{c_e^2 - M^2}{K_0} + \frac{(1 - c_e)^2 - M^2}{K_1} \tanh(\alpha K_1) = 0. \tag{4.16}$$

For the odd mode, we set $A_e = 0$, $A_+ = -A_-$ and write $c = c_o$. Then the jump conditions and (4.14) give

$$\frac{c_o^2 - M^2}{K_0} + \frac{(1 - c_o)^2 - M^2}{K_1} \coth(\alpha K_1) = 0. \tag{4.17}$$

In contrast to the vortex sheet dispersion relation (4.6), here c depends upon α.

The case $F = 0$ may be solved exactly. Then $K_{0,1} = 1$, so (4.16) and (4.17) give

$$c_e = \frac{T + \mathrm{i}\sqrt{T - M^2(1 + T)^2}}{1 + T}, \quad c_o = \frac{1 + \mathrm{i}\sqrt{T - M^2(1 + T)^2}}{1 + T}, \tag{4.18a,b}$$

where $T = \tanh\alpha$. Gedzelman (1973) gave formulae for these two cases (his (3.4) and (3.5)), but both are missing factors of 2; the case $M = 0$ was given in Rayleigh (1878). Both modes are stable for all α when $M \geqslant 1/2$; otherwise, both modes are unstable (with the same growth rate) provided that

$$M < M_c = \frac{\sqrt{T}}{1 + T} \Leftrightarrow \alpha > \alpha_c = \tanh^{-1}\left(\frac{1 - 2M^2 - \sqrt{1 - 4M^2}}{2M^2}\right). \tag{4.19}$$

Thus, the magnetic field introduces a long-wave cutoff.

For non-zero F and M, solutions to (4.16) and (4.17) exhibit a wide variety of behaviour, as described in Mak (2013). Here we focus on the long-wave regime ($\alpha \ll 1$), in which solutions exhibit fundamentally jet-like characteristics.

We consider first the even mode. Assuming that K_1 remains bounded (which may be confirmed *a posteriori*), $\tanh(\alpha K_1) \approx \alpha K_1$ when $\alpha \ll 1$, so that (4.16) becomes

$$\frac{c_e^2 - M^2}{\sqrt{1 - F^2(c_e^2 - M^2)}} + \alpha((1 - c_e)^2 - M^2) = 0. \tag{4.20}$$

Suppose that $F^2 = O(1)$. If $M = O(1)$, then $c_e = \pm M$ at leading order, and the next correction in α is also real. However, if $M^2 \sim \alpha \ll 1$, then at leading order, (4.20) gives

$$c_e \sim \pm\mathrm{i}\sqrt{\alpha - M^2} \quad \text{as } M^2 \sim \alpha \to 0,\ F^2 = O(1), \tag{4.21}$$

which is consistent with the small M and α limits of (4.18). Thus a weak magnetic field reduces the growth rate of the hydrodynamic instability and eventually suppresses it, with instability when

$$M < M_c = \alpha^{1/2}, \quad \text{or equivalently when } \alpha > \alpha_c = M^2. \tag{4.22}$$

A dependence on F appears only at the next order in α.

To capture the influence of F, the analysis may be extended to larger values of F with $F^2 \sim \alpha^{-1} \gg 1$. In this case, the square root in (4.20) also enters the balance at leading order, and we obtain

$$c_e \sim \mathrm{i}\left(\frac{\alpha^2 F^2}{2} - M^2 + \sqrt{\frac{\alpha^4 F^4}{4} + \alpha^2}\right)^{1/2} \quad \text{as } M^2 \sim F^{-2} \sim \alpha \to 0, \tag{4.23}$$

https://doi.org/10.1017/jfm.2015.718 Published online by Cambridge University Press

which formally reduces to (4.21) when F is of order unity. Again there is a long-wave cutoff due to the magnetic field, with instability only when

$$M < M_c = \frac{\alpha^2 F^2 + \sqrt{4\alpha^2 + \alpha^4 F^4}}{2} \;\Leftrightarrow\; \alpha > \alpha_c = \frac{M^2}{\sqrt{1 + M^2 F^2}}. \tag{4.24}$$

Comparing (4.22) with (4.24) shows the destabilising influence of increasing F. Indeed, in contrast to the result (4.9) for the vortex sheet, (4.23) does not predict stabilisation for large F when $\alpha \ll 1$.

Now consider the odd mode with $\alpha \ll 1$. The dispersion relation (4.17) reduces to

$$\frac{\alpha(c_o^2 - M^2)}{\sqrt{1 - F^2(c_o^2 - M^2)}} + \frac{(1 - c_o)^2 - M^2}{1 - F^2((1 - c_o)^2 - M^2)} = 0. \tag{4.25}$$

Suppose that $F^2 = O(1)$. If $M = O(1)$, then c_o is real at the first two orders in α. However, if $M^2 \sim \alpha \ll 1$, then at leading order, (4.25) gives

$$c_o \sim 1 + \mathrm{i}\left(\frac{\alpha}{\sqrt{1 - F^2}} - M^2\right)^{1/2} \quad \text{as } M^2 \sim \alpha \to 0,\ F^2 = O(1),\ 1 - F^2 = O(1). \tag{4.26}$$

When $F < 1$, again there is a cutoff due to the magnetic field, with instability only when

$$M < M_c = \frac{\alpha^{1/2}}{(1 - F^2)^{1/4}}, \quad \text{or equivalently when } \alpha > \alpha_c = M^2\sqrt{1 - F^2}. \tag{4.27}$$

These cutoffs show a strong destabilisation as $F \to 1$. When F is close to 1, the asymptotic ordering leading to (4.26) breaks down, and one must instead seek solutions with $c = 1 + O(\alpha^{2/5})$. When $F > 1$, expression (4.26) shows that c_o always has a positive imaginary part, so that there is no cutoff at small M (when $\alpha \ll 1$). So again, in contrast to the vortex sheet, there is no stabilisation at large F.

4.3. *Smooth profiles*

We now consider smooth profiles of the basic state velocity, again with uniform field and no topography. For long-wave disturbances, the leading-order instability behaviour is determined by $U(y)$ as $|y| \to \infty$, with higher-order corrections determined by the flow at finite y. Assuming that $U_\pm = U(\pm\infty)$ are well defined, the analysis reveals two distinct balances: a shear layer (if $U_+ \neq U_-$) or a jet (if $U_+ = U_-$), which are analogous to the piecewise constant profiles studied in §§ 4.1 and 4.2. On choosing an appropriate frame of reference and suitable normalisation for the basic flow, any velocity profile may thus be designated as either a shear layer with $U_\pm = \pm 1$, or as a jet with $U_\pm = 0$.

We consider the governing equation (2.7), written as

$$Z^2(G'' - \alpha^2 K^2 G) + (Z^2)'G' = 0, \quad Z^2 = \frac{S^2}{K^2}, \tag{4.28}$$

with S^2 and K^2 depending on y and c as defined by (2.6). We assume that U' (and so $(Z^2)'$) decays sufficiently rapidly as $|y| \to \infty$. Adopting the same notation as Drazin & Howard (1962), we consider solutions of the form

$$G(y) = \begin{cases} G_+(y) = \chi(y)\exp(-\alpha K_+ y), & y > 0, \\ G_-(y) = \theta(y)\exp(+\alpha K_- y), & y < 0, \end{cases} \tag{4.29}$$

https://doi.org/10.1017/jfm.2015.718 Published online by Cambridge University Press

where $K_\pm^2 = 1 - F^2 S_\pm^2 = 1 - F^2((U_\pm - c)^2 - M^2)$. The perturbations must decay as $|y| \to \infty$; hence $\mathrm{Re}\,(K_\pm) > 0$. We consider expansions of the form

$$\chi(y) = \sum_{n=0}^{\infty} (+\alpha)^n \chi_n(y), \quad \theta(y) = \sum_{n=0}^{\infty} (-\alpha)^n \theta_n(y), \tag{4.30a,b}$$

with $\chi_0, \theta_0 \to$ const. $(\neq 0)$ and $\chi_n, \theta_n \to 0$ as $|y| \to \infty$ $(n \geqslant 1)$. It turns out to be most convenient to fix $\chi_0(\infty) = \theta_0(-\infty) = 1$, and then to accommodate the necessary degree of freedom in the matching conditions for G at $y = 0$, namely $G_+(0) = \Gamma G_-(0)$ and $G'_+(0) = \Gamma G'_-(0)$ for some constant Γ. Consistency thus implies

$$G_+(0) G'_-(0) = G_-(0) G'_+(0). \tag{4.31}$$

Without loss of generality, we shall focus on the equations for χ; those for θ follow in a similar fashion. On substituting (4.29) (with (4.30)) into (4.28), equating the coefficients at each order of α gives

$$0 = (Z^2 \chi_0')', \tag{4.32a}$$

$$0 = (Z^2 \chi_1')' - K_+(2Z^2 \chi_0' + (Z^2)' \chi_0), \tag{4.32b}$$

$$0 = (Z^2 \chi_{n+2}')' - K_+(2Z^2 \chi_{n+1}' + (Z^2)' \chi_{n+1}) + Z^2(K_+^2 - K^2)\chi_n, \quad n \geqslant 0. \tag{4.32c}$$

Equation (4.32*a*) integrates to $Z^2 \chi_0' = C$, with the conditions at infinity then giving $C = 0$. Thus $\chi_0 = \text{const.} = 1$ through our choice of $\chi_0(\infty)$. Integration of (4.32*b*,*c*) then gives, after some algebra,

$$\left.\begin{aligned} \chi_1 &= \int_\infty^y \left(1 - \frac{Z_+^2}{Z^2(y_1)}\right) \mathrm{d}y_1, \\ \chi_2 &= \int_\infty^y \left(\frac{1}{Z^2(y_1)} \int_\infty^{y_1} (S^2(y_2) - S_+^2)\, \mathrm{d}y_2 + K_+^2 \int_\infty^{y_1} \left(1 - \frac{Z_+^2}{Z^2(y_2)}\right) \mathrm{d}y_2 \right) \mathrm{d}y_1. \end{aligned}\right\} \tag{4.33}$$

The matching condition (4.31) then leads to the result

$$\begin{aligned} 0 \;=\; & \left(\frac{S_+^2}{K_+} + \frac{S_-^2}{K_-}\right) + \alpha \left(\int_0^\infty (S^2 - S_+^2)\, \mathrm{d}y + \int_{-\infty}^0 (S^2 - S_-^2)\, \mathrm{d}y \right. \\ & \left. - \frac{S_+^2}{K_+ K_-} \int_{-\infty}^0 \left(1 - \frac{S_-^2}{S^2}\right) \mathrm{d}y - \frac{S_-^2}{K_+ K_-} \int_0^\infty \left(1 - \frac{S_+^2}{S^2}\right) \mathrm{d}y \right) + O(\alpha^2). \end{aligned} \tag{4.34}$$

On expressing the eigenvalue c as $c = c^{(0)} + \alpha c^{(1)} + \alpha^2 c^{(2)} + \cdots$, (4.34) then determines the successive $c^{(j)}$.

Although we have focused on the case of a uniform magnetic field, it is possible to include a non-uniform field, subject to imposing conditions analogous to those for $U(y)$. With underlying topography, other assumptions on $H(y)$ are required, as described by Collings & Grimshaw (1980).

4.3.1. *Shear layers*

For a shear layer, $U_\pm = \pm 1$, and the leading-order term of expression (4.34) gives

$$\frac{(1 - c^{(0)})^2 - M^2}{\sqrt{1 - F^2((1 - c^{(0)})^2 - M^2)}} + \frac{(1 + c^{(0)})^2 - M^2}{\sqrt{1 - F^2((1 + c^{(0)})^2 - M^2)}} = 0. \tag{4.35}$$

https://doi.org/10.1017/jfm.2015.718 Published online by Cambridge University Press

This is exactly the eigenvalue equation of the vortex sheet (4.6); hence, for any shear layer, $c \to c_v$, as defined in (4.8), as $\alpha \to 0$. This is not surprising; sufficiently long waves see the shear layer as a discontinuity in the flow.

When $F > F_c$, as defined in (4.9), c_v is real. However there could be an instability at higher order. Following Blumen, Drazin & Billings (1975), we may calculate $c^{(1)}$, although this requires $U(y)$ to be specified. Such a calculation is performed in § 5.1.3 for $U(y) = \tanh y$, revealing a secondary instability for large values of F.

4.3.2. *Jets*

For a jet, $U_\pm = 0$; at leading order the flow is thus seen to be uniform and hence there is no instability. It is therefore essential to retain the $O(\alpha)$ terms in (4.34), which becomes

$$0 = \frac{2S_0^2}{K_0} + \alpha\left(\int_{-\infty}^{\infty}(S^2 - S_0^2)\,\mathrm{d}y - \frac{S_0^2}{K_0^2}\int_{-\infty}^{\infty}\left(1 - \frac{S_0^2}{S^2}\right)\mathrm{d}y\right) + O(\alpha^2), \tag{4.36}$$

where $S_0^2 = (0-c)^2 - M^2$, $K_0^2 = 1 - F^2 S_0^2$. Here, for a fixed value of F, we need to consider different regimes for M.

For $F^2 = O(1)$, if $M^2 = O(1)$ then $c^{(0)}$ and $c^{(1)}$ are real. To find an instability we need to consider the regime $M^2 \sim \alpha$, which implies $c^{(0)} = 0$. At the next order, we choose to balance the first two terms on the right-hand side of (4.36), assuming that the second integral is negligible; this is confirmed by the analysis of appendix A. Defining $E = \int_{-\infty}^{+\infty} U^2/2\,\mathrm{d}y$, where U is assumed to decay sufficiently rapidly that E is finite, we obtain

$$c \sim \mathrm{i}\sqrt{\alpha E - M^2} \quad \text{as } M^2 \sim \alpha \to 0,\ F^2 = O(1). \tag{4.37}$$

The corresponding result for compressible hydrodynamics was derived by Gill & Drazin (1965), and for incompressible MHD by Gedzelman (1973).

For large F, the regime of interest is $M^2 \sim \alpha$, $F^2 \sim \alpha^{-1}$. Considering the same balance as above gives

$$c \sim \mathrm{i}\left(\frac{\alpha^2F^2E^2}{2} - M^2 + \sqrt{\alpha^2E^2 + \frac{\alpha^4F^4E^4}{4}}\right)^{1/2} \quad \text{as } F^{-2} \sim M^2 \sim \alpha \to 0. \tag{4.38}$$

This result reduces to (4.37) in the limit of small F. The presence of a magnetic field introduces a long-wave cutoff.

Note that expressions (4.37) and (4.38) take the same form as (4.21) and (4.23), found for the even mode of the rectangular jet. Indeed, if we take $U(y)$ defined by (4.13), then $E = 1$ and the correspondence is exact. The discussion of the rectangular jet concerning long-wave cutoffs and destabilisation at large F thus applies to arbitrary smooth jets for $\alpha \ll 1$.

Interestingly, the dispersion relation (4.26) for the odd mode of the rectangular jet is not captured by the long-wave analysis. The reason is that, for these modes, c_r remains $O(1)$ as $\alpha \to 0$ (as in (4.26)). This leads to a problem in (4.28) since, when $M^2 \sim \alpha$, Z^2 becomes small when $U \approx c_r$, and the standard asymptotic procedure leading to (4.32) breaks down. In the hydrodynamic case it is found that $c_i \sim \alpha^{2/3}$ (Drazin & Howard 1962); our numerical results suggest the same scaling when F and M are non-zero.

https://doi.org/10.1017/jfm.2015.718 Published online by Cambridge University Press

5. Instability of smooth profiles at finite wavenumber

Having identified the existence of two classes of flows for instability at small wavenumbers, we now consider how these instabilities extend to finite wavenumber. We consider one smooth shear layer (the hyperbolic tangent profile) and one smooth jet (the Bickley jet). Linear instability calculations involving these two profiles are well documented in a wide variety of contexts (e.g. Lipps 1962; Howard 1963; Michalke 1964; Sutherland & Peltier 1992; Hughes & Tobias 2001) and these provide a comparison and check on our results. We again restrict attention (for simplicity) to the case of a uniform background magnetic field, $B(y) \equiv 1$, and with no underlying topography, $H(y) \equiv 1$. Even so, the eigenvalue problem (2.7) must be solved numerically; we employ a shooting method with a continuation approach, as detailed in appendix B.

5.1. *Hyperbolic-tangent shear layer*

In this subsection, we consider the basic state velocity defined by

$$U(y) = \tanh y. \tag{5.1}$$

5.1.1. *General instability characteristics*

From inequality (3.3) we know that the growth rates αc_i are bounded above by $|U'|_{max}/2 = 1/2$; furthermore, from the stability criteria (3.11) or (3.12), this profile is stable when $M \geqslant 1$. When $F = M = 0$, instability exists only when $0 < \alpha < 1$, with a neutral mode at $\alpha = 1$ (Drazin & Reid 1981, § 31.10). In this case, there is a single primary mode of instability, which may be classified as an inflection-point instability and attributed to interacting waves supported by the background shear (see, for example, the review by Carpenter *et al.* 2012). When $M = 0$, but $F \neq 0$, there is a secondary mode of instability, first found by Blumen *et al.* (1975) for two-dimensional compressible hydrodynamics. This has a smaller growth rate and a less pronounced spatial decay than the primary mode. Further, whilst the primary mode has $c_r = 0$, there are two branches for the secondary mode with equal and opposite (non-zero) phase speeds, consistent with the parity results in § 3.3, which ensure that $c = \pm c_r + \mathrm{i}c_i$ for unstable modes. The secondary mode can be attributed to interacting gravity waves (e.g. Satomura 1981; Hayashi & Young 1987; Takehiro & Hayashi 1992; Balmforth 1999) and, indeed, can occur for linear shear flows, explicitly filtering out the possibility of waves due to a background vorticity gradient. This is consistent with the theorem of Ripa (1983), which states that for instability (with $M = 0$), either the associated potential vorticity profile possesses an inflection point, or $F > 1$, both of which encourage instability through interacting waves.

Both modes have been found in our SWMHD system. Figure 3 shows contours of c_i over (M, F) space at selected values of α for the profile (5.1), distinguishing between the primary mode (with $c_r = 0$, shown as solid contours) and the secondary mode (with $c_r \neq 0$, shown as dashed contours). In figure 3(*a*), at $\alpha = 0.7$, and figure 3(*b*), at $\alpha = 0.44$ (which is the most unstable mode when $F = M = 0$ (Michalke 1964)), only the primary mode exists. In figure 3(*c*), at $\alpha = 0.2$, and figure 3(*d*), at $\alpha = 0.01$, both modes exist, although in different parts of (M, F) space. We observe that figure 3(*d*) and figure 1 are remarkably similar, confirming the results from the long-wave asymptotic analysis in § 4.

The growth rate αc_i is shown in figure 4 as a function of α; secondary modes generally have weaker growth rates than the primary modes, consistent with the results

https://doi.org/10.1017/jfm.2015.718 Published online by Cambridge University Press

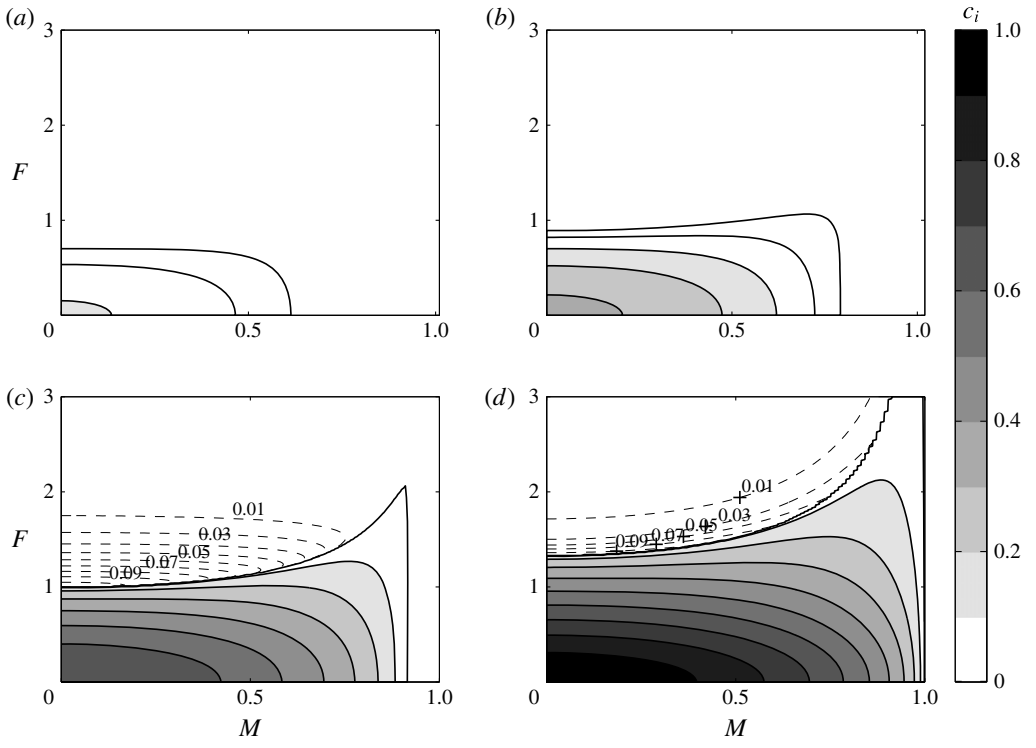


FIGURE 3. Contours of c_i over (M, F) space for $U(y) = \tanh y$; (a) $\alpha = 0.70$, (b) $\alpha = 0.44$, (c) $\alpha = 0.20$, (d) $\alpha = 0.01$. The primary modes (here classified by $|c_r| < 10^{-3}$) are contoured as solid lines. The secondary modes are contoured as dashed lines.

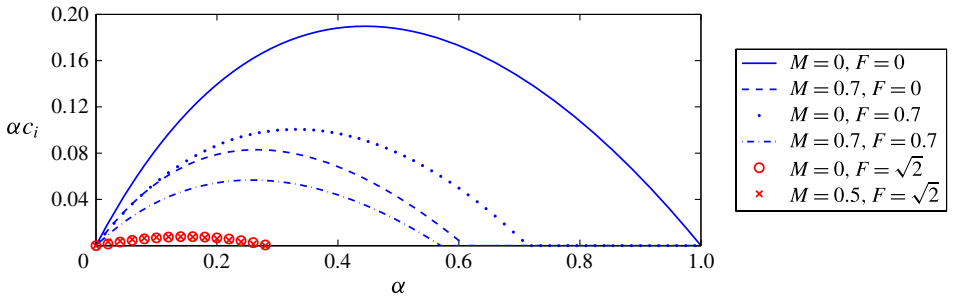


FIGURE 4. (Colour online) Growth rate versus α at selected parameter values for $U(y) = \tanh y$. The upper four curves are primary modes, the lower two are secondary modes.

of Blumen *et al.* (1975). As we shall see in § 5.1.3, where we extend the long-wave asymptotic analysis beyond the leading order, the relation between the two types of unstable modes can be explored in some detail in the long-wavelength limit.

5.1.2. *Instability mechanism of the primary mode*

As mentioned above, inflection-point instabilities can be attributed to interacting waves supported by the vorticity gradient of the background shear. These waves are

https://doi.org/10.1017/jfm.2015.718 Published online by Cambridge University Press

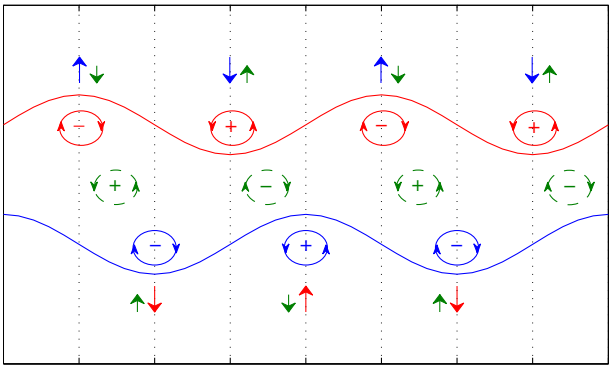


FIGURE 5. (Colour online) Modified counter-propagating Rossby wave mechanism in schematic form. Shown are two displaced material contours. The associated vorticity anomalies when $F = M = 0$ are shown by the closed solid curves; the effect of these on the other contours, leading to instability, is shown by the longer arrows. The closed dashed curves represent the additional vorticity anomalies when F and M are non-zero. The stabilising effect of these, which opposes the driving of the instability, is shown by the shorter arrows.

normally called Rossby waves, although they should not be confused with Rossby waves that could arise from a background vorticity gradient due to planetary rotation. The constructive interference of a pair of counter-propagating Rossby waves has been proposed as the mechanism leading to instability of shear flows in a variety of settings (e.g. Bretherton 1966; Hoskins, McIntyre & Robertson 1985; Caulfield 1994; Harnik & Heifetz 2007; Heifetz *et al.* 2015). For the SWMHD system, it is therefore natural to enquire how this underlying mechanism is modified by magnetic and shallow-water effects.

Let us first consider the case of $F = M = 0$. The background vorticity profile, shown in figure 5, supports two Rossby waves, propagating in the negative (positive) x-direction on the positive (negative) vorticity gradient in $y > 0$ ($y < 0$). Viewed individually, the Rossby waves are neutral and propagate against the mean flow. If, however, they become phase locked, they can interfere constructively, leading to mutual amplification and hence instability. This is shown schematically in figure 5, where the two Rossby waves are represented as perturbed vorticity contours (or equivalently perturbed material contours) for $y > 0$ and $y < 0$. The resulting positive and negative vorticity anomalies are also shown. In this configuration, the transverse flow induced by each wave acts to amplify the existing transverse material displacement of the other. There is thus a mutual amplification and instability. This is also consistent with numerical solutions for instabilities of the flow (5.1) when $F = M = 0$; figure 6(a) shows the vorticity perturbation of the most unstable mode (with $\alpha = 0.44$), in agreement with figure 5.

We now quantify how free-surface and magnetic effects modify this mechanism for SWMHD. We use the SWMHD vorticity equation, which is given by

$$\frac{\mathrm{D}\omega}{\mathrm{D}t} \equiv \frac{\partial \omega}{\partial t} + \boldsymbol{u}\cdot\boldsymbol{\nabla}\omega = -(\boldsymbol{\nabla}\cdot\boldsymbol{u})\omega + M^2\boldsymbol{B}\cdot\boldsymbol{\nabla}j + M^2(\boldsymbol{\nabla}\cdot\boldsymbol{B})j, \tag{5.2}$$

where ω and j are the z-components of the vorticity and electric current. Linearising about the basic state $\boldsymbol{U}_0 = U(y)\boldsymbol{e}_x$, $\boldsymbol{B}_0 = \boldsymbol{e}_x$, taking modal solutions of the form (2.4)

https://doi.org/10.1017/jfm.2015.718 Published online by Cambridge University Press

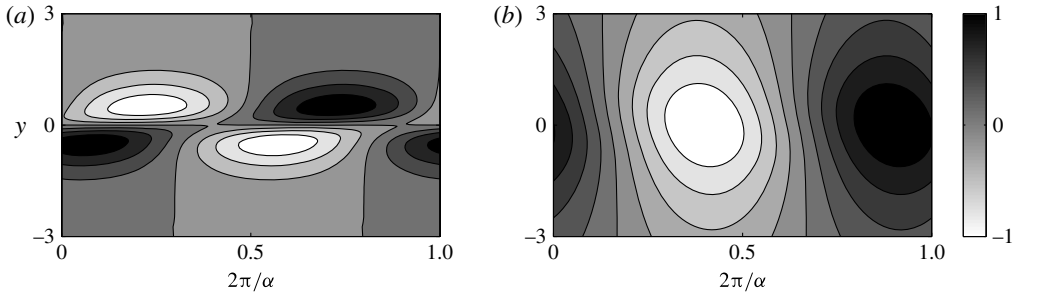


FIGURE 6. Eigenfunctions of (*a*) vorticity and (*b*) height for the most unstable modes for $U(y) = \tanh y$ at $F = 0$, $M = 0$.

and noting that $v = (\partial/\partial t + U\partial/\partial x)\eta$, where η is the cross-stream displacement, we obtain the vorticity budget

$$\omega = -\eta\Omega' + F^2 h\Omega + M^2 \frac{j}{U - c}, \tag{5.3}$$

where $\Omega = -U'$ is the basic state vorticity. The three contributions to ω arise from the advection of the background vorticity, vortex stretching in shallow water, and magnetic tension.

Inspection of figure 3 shows that the instability is most vigorous when $F = M = 0$; we therefore expect that the vorticity anomalies from the magnetic and shallow-water effects will be stabilising. The vorticity ω and the decomposition (5.3) are shown in figure 7 for a mode at $F = 0.5$, $M = 0.25$. Even though this eigenfunction results from a calculation with non-zero F and M, the $-\eta\Omega'$ contribution has the same structure as that of figure 6(*a*). The extra contributions from non-zero F and M are shown in figure 7(*c*,*d*); both of these terms are maximised at $y = 0$, where they are approximately in phase. Thus, at the simplest level, they lead to the vorticity anomalies shown by the dashed circles in figure 5. The transverse flow induced by these vorticity anomalies counteracts the mutually amplifying transverse flow of the Rossby waves, and is thus stabilising; a similar observation has been made for hydrodynamic stratified flows by Rabinovich *et al.* (2011) and for incompressible MHD by Heifetz *et al.* (2015).

As a further verification of these ideas, we have also adopted a perturbative approach to the analysis of expression (5.3), approximating the shallow-water and magnetic contributions using the eigenfunction for $F = M = 0$. It can be seen that calculating $F^2 h\Omega$ using h in figure 6(*b*) is consistent with the vorticity anomaly from the full linear equations (figure 7*c*). To obtain an estimate of the magnetic contribution, it is necessary to calculate j using the governing equations (2.3) with the velocity obtained when $F = M = 0$. This is slightly more involved than for h, but can be shown to provide a vorticity anomaly consistent with figure 7(*d*) (see Mak 2013).

5.1.3. *Long-wave asymptotics for the secondary mode*

We can gain some understanding of the secondary mode, and its connection to the primary mode, by considering the limit $\alpha \ll 1$. The mathematical framework was developed in § 4.3.1, where an expression c_v was obtained for the leading-order phase

https://doi.org/10.1017/jfm.2015.718 Published online by Cambridge University Press

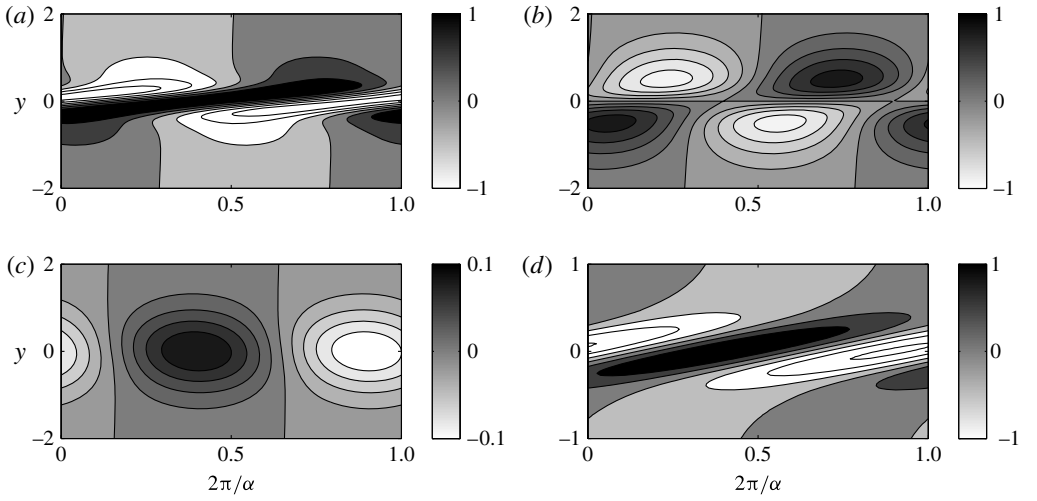


FIGURE 7. A generic vorticity budget breakdown for the case where neither F nor M is zero; shown here is $F=0.5$ and $M=0.25$, with (*a*) ω, (*b*) $-\eta\Omega'$, (*c*) $F^2h\Omega$, (*d*) $M^2j/(U-c)$. Notice that the vorticity contribution from the magnetic term is substantially larger than that from the shallow-water term.

speed $c^{(0)}$, which, as noted, is real for $F > F_c$. In this case, following Blumen *et al.* (1975), we use expression (4.34) to calculate $c^{(1)}$, the next term in the expansion of the eigenvalue. For the particular flow (5.1), and after considerable algebra (Mak 2013), we obtain

$$c^{(1)} = \mathrm{i}\frac{\sqrt{F^2((1-c_v)^2-M^2)-1}}{4c_v^2}\frac{(1+c_v)^2-M^2}{\sqrt{1+4F^2+4F^4M^2}} \times\left(1+\frac{c_v}{2}\left(\log\left(\frac{(1+c_v)^2-M^2}{(1-c_v)^2-M^2}\right)-\delta_1-\delta_2\right) +\frac{1-M^2-c_v^2}{4M}\left[\log\left(\frac{(1+M)^2-c_v^2}{(1-M)^2-c_v^2}\right)+\delta_1-\delta_2\right]\right), \tag{5.4}$$

where $\delta_1=\delta_2=0$ when $F<F_c$, and where

$$\delta_1=\begin{cases}\pi\mathrm{i}, & |c_v-M|\leqslant 1,\\ 0, & \text{otherwise},\end{cases}\qquad \delta_2=\begin{cases}\pi\mathrm{i}, & c_v+M\leqslant 1,\\ 0, & \text{otherwise},\end{cases} \tag{5.5a,b}$$

when $F>F_c$ for the root with $c^{(0)}=c_v>0$ (there are corresponding expressions for the other root with $c^{(0)}=-c_v<0$). It may be shown that for $M\to 0$, the expression inside the square brackets is equal to $4M(1-c_v)^{-2}+O(M^2)$, and that (5.4) is equivalent to equation (21) in Blumen *et al.* (1975). For sufficiently large F, $\mathrm{Im}\,(c^{(1)})>0$; this is the weak secondary instability. By expanding c_v up to powers of F^{-4}, it may be shown from (5.4) that $\mathrm{Im}\,(c^{(1)})\downarrow 0$ as $F\to\infty$, so there is no cutoff at finite F.

The analysis leading to expression (5.4) is valid only when c_v is not small, i.e. for F^2 not close to $F_c^2=2(1-M^2)^{-1}$ or M not close to 1. When $F^2-F_c^2$ is small, $O(\alpha^{2/3})$

https://doi.org/10.1017/jfm.2015.718 Published online by Cambridge University Press

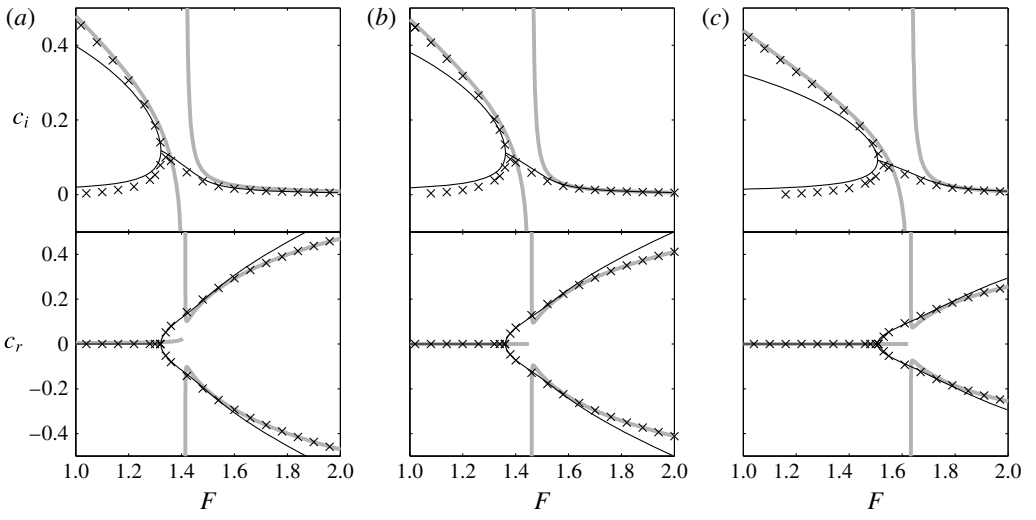


FIGURE 8. Transition from the primary to secondary mode for $U(y) = \tanh y$. Shown are c_i and c_r versus F at $\alpha = 0.01$ for (*a*) $M = 0$, (*b*) $M = 0.25$, (*c*) $M = 0.5$. The crosses are the numerical results, the grey lines show the outer expansion $c_v + \alpha c^{(1)}$, with $c^{(1)}$ given by (5.4), and the black lines the inner expansion given by relevant solutions to the cubic equation (5.6). For $F > F_{cusp}$, solutions with both $c_r > 0$ and $c_r < 0$ are shown.

to be precise, we have $c_v \sim \alpha c^{(1)} \sim \alpha^{1/3}$. Rescaling and choosing the appropriate branch so that $\mathrm{Re}\,(\sqrt{\cdots}) > 0$ gives $c^{(1)}$ as the solution of the cubic equation

$$\frac{6+2M^2}{(1-M^2)^3}(c^{(1)})^3 + (F_c^2 - F^2)c^{(1)} - \mathrm{i}\alpha\left(\frac{1}{1-M^2} + \frac{1}{2M}\log\frac{1+M}{1-M}\right) = 0, \tag{5.6}$$

for $\alpha^{2/3} \sim 2(1-M^2)^{-1} - F^2 \to 0$. When $M = 0$, (5.6) reduces to equation (23) in Blumen *et al.* (1975). There are two admissible roots with positive imaginary parts. There is a transition to non-zero real parts when

$$F^2 = F_{cusp}^2 = \frac{2}{1-M^2} - 3\left(\frac{\alpha^2}{4}\frac{6+2M^2}{(1-M^2)^3}\left(\frac{1}{1-M^2} + \frac{1}{2M}\log\frac{1+M}{1-M}\right)^2\right)^{1/3}. \tag{5.7}$$

This expression reduces to $F_{cusp}^2 = 2 - 3(6\alpha^2)^{1/3}$ when $M \to 0$, as given by Blumen *et al.* (1975).

The asymptotic results, together with the numerical computations, are presented in figure 8. The inner expansion, including the location of the cusp given by (5.7), is in good agreement when $F \approx F_c$, and the outer expansion is in good agreement otherwise. Note that the inner expansion establishes the existence of two unstable modes when $F < F_{cusp}$, whereas the outer expansion only picks up the mode with larger c_i, i.e. the primary mode. It is the coalescence of the two modes revealed by the inner expansion that leads to the pair of secondary unstable modes. Thus the primary and secondary modes are continuously connected, but in a non-trivial manner.

5.2. *Bickley jet*

In this subsection we consider the basic state velocity defined by

$$U(y) = \mathrm{sech}^2 y. \tag{5.8}$$

https://doi.org/10.1017/jfm.2015.718 Published online by Cambridge University Press

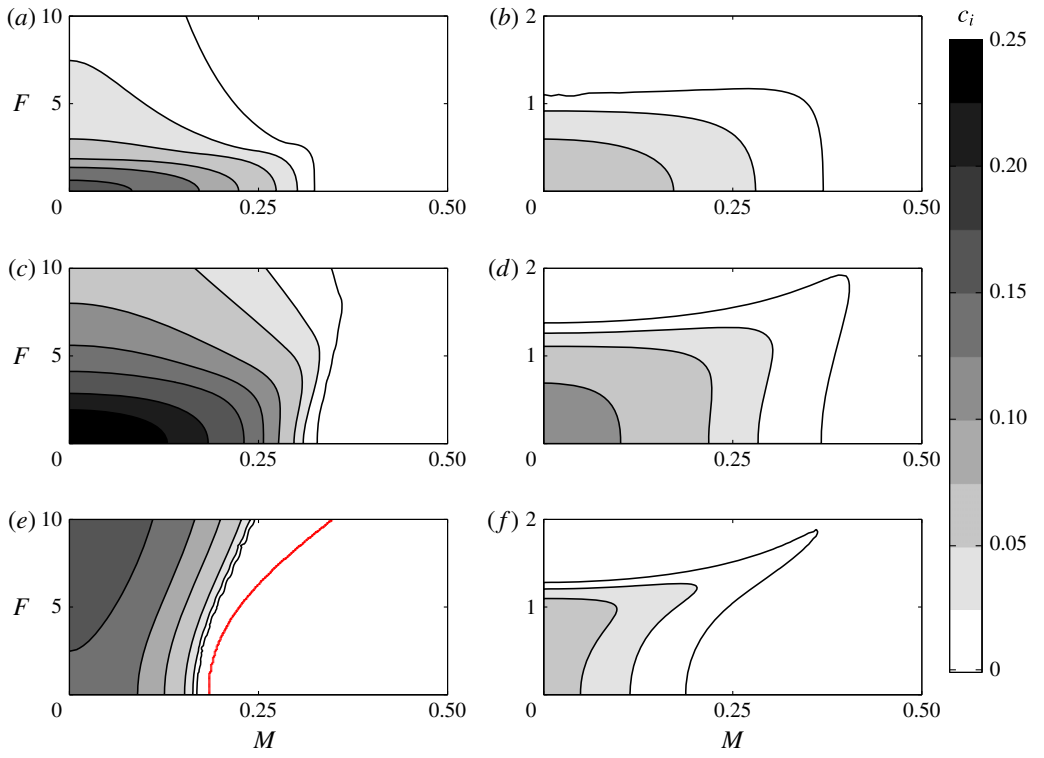


FIGURE 9. (Colour online) Contours of c_i over (M, F) space at selected α for the even (a,c,e) and odd (b,d,f) modes of the Bickley jet, with (a) $\alpha = 0.9$, (b) $\alpha = 0.52$, (c) $\alpha = 0.3$, (d) $\alpha = 0.23$, (e,f) $\alpha = 0.05$. The cutoff from the asymptotic result (5.10) is also plotted in red in (e).

From inequality (3.3), the growth rate αc_i is bounded above by $|U'|_{max}/2 = 2/(3\sqrt{3})$; furthermore, from stability criterion (3.12), this flow is stable when $M \geqslant 1/2$. The Bickley jet is even about $y = 0$ and hence the parity result of § 3.3 holds – i.e. the eigenfunctions are either even or odd. In this case, the numerical method in appendix B may be adapted to integrate over only half the domain, with the imposition of either $G'(0) = 0$ (even mode) or $G(0) = 0$ (odd mode).

When $F = M = 0$ there is a single even mode and a single odd mode, which are unstable only in the respective bandwidths $0 < \alpha < 2$ and $0 < \alpha < 1$ (Drazin & Reid 1981, § 31.9). Figure 9 shows contours of c_i for the continuation of these modes over (M, F) space for selected values of α. The values of α correspond to: (i) the most unstable mode when $F = M = 0$ (a,b); (ii) the mode with highest c_i when $F = M = 0$ (c,d); (iii) a long-wave disturbance (e,f). Increasing F and M is generally stabilising; however, there are small regions where this does not hold, as can be seen from figure 9(d,f). Figure 10 shows the growth rate as a function of α for selected values of F and M. The short-wave cutoffs, which for $F = M = 0$ are at $\alpha = 2$ (even mode) and $\alpha = 1$ (odd mode), are reduced as M increases, with a non-trivial dependence on F.

The behaviour at small α can be clarified using the long-wave analysis of § 4.3.2, although, as discussed there, this holds only for the even mode. Noting that for the

https://doi.org/10.1017/jfm.2015.718 Published online by Cambridge University Press

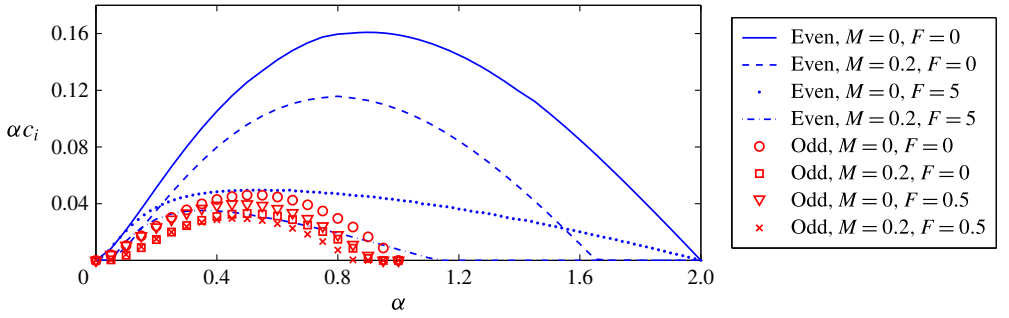


FIGURE 10. (Colour online) Instability of the Bickley jet: growth rate of the mode tracked from $F=M=0$.

Bickley jet, $2E=\int_{-\infty}^{+\infty}(\mathrm{sech}^2 y)^2\,\mathrm{d}y=4/3$, the long-wave asymptotic results (4.37) and (4.38) become

$$c\sim \mathrm{i}\sqrt{\tfrac{2}{3}\alpha-M^2}\quad\text{as } M^2\sim\alpha\to 0,\ F^2=O(1), \tag{5.9}$$

and

$$c\sim \mathrm{i}\left(\frac{2}{9}\alpha^2F^2-M^2+\frac{2}{3}\sqrt{\alpha^2+\frac{\alpha^4F^4}{9}}\right)^{1/2}\quad\text{as } F^{-2}\sim M^2\sim\alpha\to 0. \tag{5.10}$$

There is a long-wave cutoff due to the magnetic field (cf. (4.24)). The accuracy of this is verified in figure 11, which shows the comparison between the numerically determined growth rates and the asymptotic results (5.9) and (5.10). As discussed in § 4.3.2, the long-wave analysis does not capture the odd mode since c_r remains $O(1)$ as $\alpha\to 0$. This has been verified numerically, where it is found that $c_i\sim\alpha^{2/3}$, a result derived for the hydrodynamic case by Drazin & Howard (1962).

As discussed above, when $M=0$ the instability problem is equivalent to that of two-dimensional compressible hydrodynamics. There it is known that the rectangular jet supports multiple modes of instability at sufficiently large Mach number (here corresponding to sufficiently large F), which are due to over reflexion (Gill 1965). It is therefore natural to ask if there are corresponding instabilities for the smooth Bickley jet profile and, if so, how they may change when M is non-zero. We have performed a scan over (M,F) space at various values of α, with initial guesses for c within the semi-circle (3.10), solving the governing eigenvalue equation with no parity imposed. We do indeed find multiple modes of instability, with a quantised character suggestive of over reflexion, for large F when α is sufficiently large. Sample plots of c_i and cross-sections of the eigenfunctions for the even modes are shown in figure 12; the results for the odd mode are similar. As F increases, the mode tracked from $F=0$ changes character, turning into the most unstable quantised mode; furthermore, additional modes appear, although the growth rates are small.

There are two distinctive features of the spatial structure of the eigenfunctions, as shown in figure 12(*c–e*). First, there is a core region consisting of approximately quantised oscillations: the mode tracked from $F=0$ has one oscillation, the nth additional mode has $n+1$ oscillations. Second, the boundary of the core region is approximately located where $U(y)=c_r$. Here the eigenfunctions are highly oscillatory and of larger amplitude, although they are well resolved in the numerics underlying figure 12(*c–e*).

https://doi.org/10.1017/jfm.2015.718 Published online by Cambridge University Press

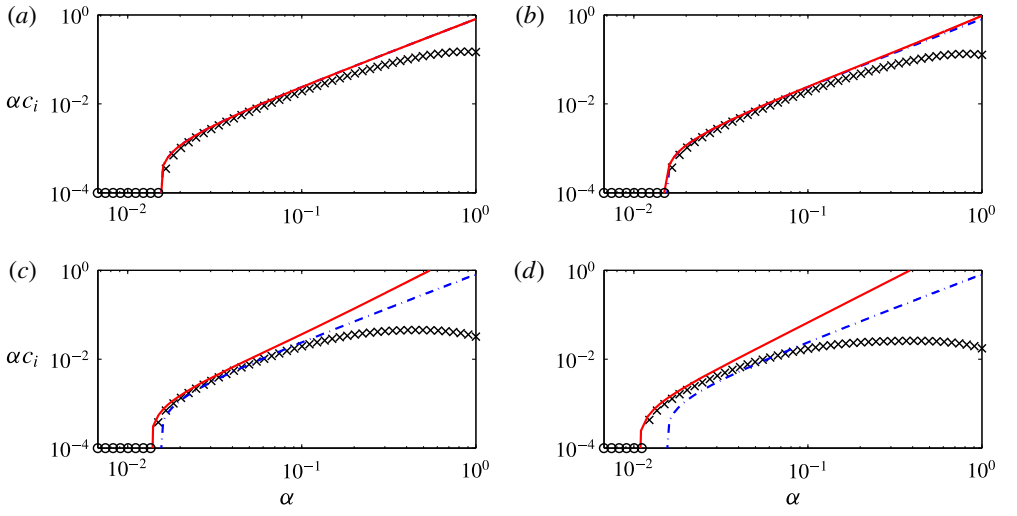


FIGURE 11. (Colour online) Comparison of the computed growth rates for the even modes (crosses; circles denote solutions with zero growth rates) and the predicted growth rates from the asymptotic results (5.9) and (5.10) (dot-dashed line and dashed line respectively), for $U(y) = \mathrm{sech}^2 y$. Here, $M = 0.1$, and (*a*) $F = 0$, (*b*) $F = 1$, (*c*) $F = 5$, (*d*) $F = 10$.

6. Conclusions and discussion

The SWMHD equations, introduced by Gilman (2000), are a useful model for studying MHD in thin stratified fluid layers. We have investigated the linear instability of parallel shear flows with an aligned magnetic field in planar geometry with no background rotation. The instability of hydrodynamic shear flows is a classical problem, with well-known results such as Rayleigh's inflection point criterion, Howard's semi-circle theorem and Høiland's growth-rate bound, supplemented by extensive asymptotic and numerical results for various idealised flows. Motivated by geophysical and astrophysical considerations, previous authors have extended separately the analysis to include the influence of shallow-water dynamics and a magnetic field. Here, for the first time, we have applied this classical approach to the SWMHD system, complementing previous work on the instability of specific flow configurations in spherical geometry (Gilman & Dikpati 2002; Dikpati *et al.* 2003). In our analysis, the stratification is measured by the Froude number F, while the imposed field strength is measured by the parameter M.

In § 3, we consider the stability of arbitrary flow and field profiles, leading to a growth-rate bound, semi-circle theorems and explicit stability criteria. In these, increasing M is generally stabilising. However, none of the criteria involve F, and so it is not possible to explore the combined effects of varying F and M.

One way to address these combined effects for quite general flows is via a long-wave analysis ($\alpha \ll 1$). In § 4 we generalise to SWMHD the asymptotic approach of Drazin & Howard (1962), in which all flows may be classified as either shear layers or jets. These possess contrasting instabilities. For the shear-layer profile, a key finding is that, although increasing F or M in the absence of the other is seen to be stabilising, their combined effects can offset each other, resulting in a tongue of instability for arbitrarily large F and M approaching unity. However, the strongest instabilities, with phase speeds of order unity, are found at smaller F and M. In contrast, for jets the

https://doi.org/10.1017/jfm.2015.718 Published online by Cambridge University Press

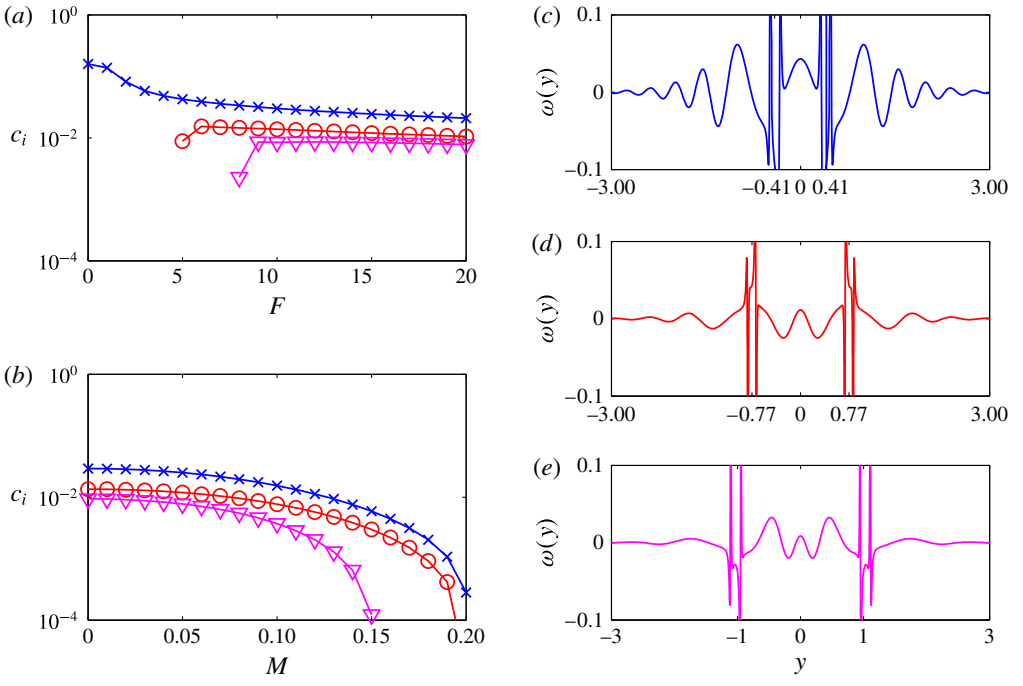


FIGURE 12. (Colour online) Even mode of the Bickley jet at $\alpha = 1$. (*a*) c_i as a function of F at $M = 0$, $\alpha = 1$. (*b*) c_i as a function of M at $F = 20$. Crosses, circles and triangles show the three most unstable modes. (*c–e*) Cross-sections of the vorticity perturbation for $F = 20$, $M = 0.05$, for these three modes. The locations where $U = c_r$ are labelled on the axes. The spikes reach an amplitude of approximately 0.5; the vertical axis has been chosen in order that the oscillations within the core are clearly visible.

phase speed is $O(\alpha^{1/2})$, so the instabilities are weaker. Also, whereas for shear layers the leading-order phase speed is independent of α, for jets it is α-dependent. There is a long-wave cutoff when M is non-zero, although this disappears with increasing F.

The interesting combined effects of F and M revealed by the long-wave analysis lead naturally to a numerical investigation of two canonical smooth flows at finite wavenumbers (§ 5). For the hyperbolic-tangent shear layer there are two modes of instability, a stronger primary mode and a weaker secondary mode, which are, respectively, extensions of inflection point and supersonic instabilities. We interpret the primary instability in terms of the counter-propagating Rossby waves (CRWs) mechanism, which has frequently been used to understand hydrodynamic shear instabilities (e.g. Carpenter *et al.* 2012). Here we show that the vorticity anomalies associated with shallow-water effects and magnetic tension oppose those for the underlying CRW mechanism; these ideas, first discussed in Mak (2013), are consistent with the later results of Heifetz *et al.* (2015) for incompressible MHD. For the Bickley jet, the symmetry of the basic state flow implies the existence of competing even and odd modes of instability. Both even and odd modes have long- and short-wave cutoffs; in between, the even mode is generally more unstable. Note that the odd mode is not picked up by the long-wave analysis, as discussed in § 4.3.2. At large F, there are multiple modes of instability, due to over reflexion.

Given the motivation for this study, it is important to consider the implications of our results for the solar tachocline. For local shear zones, with characteristic length

https://doi.org/10.1017/jfm.2015.718 Published online by Cambridge University Press

scale $L_0 = 0.1R_\odot$ and characteristic velocity $U_0 = 20$ m s^{-1}, taking 10^3 G $\lesssim B_0 \lesssim 10^5$ G gives $0.3 \lesssim M \lesssim 30$. Thus only for the weakest fields in this range will there be instability. For planetary-scale shear flows, with $L_0 = R_\odot$ and $U_0 = 200$ m s^{-1}, we have $0.03 \lesssim M \lesssim 3$ and $F \approx 0.04$. Here instability is suppressed only by fields at the strong end of the possible spectrum. The e-folding time for an instability is given by $\hat{t} = (\alpha c_i)^{-1}(L_0/U_0)$, which, for both local and planetary shears, gives $\hat{t} = O(10^6(\alpha c_i)^{-1})$ s. With $\alpha c_i \approx 0.1$, for both shear layers and jets (see figures 4 and 10), $\hat{t} = O(10^7)$ s. Since $\alpha = O(1)$ for the unstable modes, the length scale of any instability is comparable to that of the shear.

Having investigated the quite complicated behaviour that results from our idealised model, there are several natural extensions of our study. Perhaps the most important additional effect would be the inclusion of background rotation. For solar dynamics, for which we have estimated an instability time scale of $O(10^7)$ s, i.e. several solar days, we might expect rotation to modify the instabilities. In the extreme case of strong rotation, some of these effects may be similar to those of Gilman (1967), who considered quasi-geostrophic baroclinic instabilities in a thin MHD layer. Although the formulation of the problem considered here, together with the general stability criteria of § 3, does allow for non-uniform magnetic fields, all our detailed calculations have assumed the magnetic field to be uniform. Thus we have not explored the possibility of non-uniform fields destabilising hydrodynamically-stable velocity profiles, as has been studied in two-dimensional incompressible MHD (Stern 1963; Chen & Morrison 1991) and spherical SWMHD (Gilman & Dikpati 2002; Dikpati *et al.* 2003). Combining the effects of rotation and non-uniform fields would allow a direct comparison with previous studies of the solar tachocline, where the main emphasis was on the destabilisation of hydrodynamically-stable velocity profiles by non-uniform toroidal fields (Gilman & Cally 2007). Finally, the nonlinear evolution of these types of shear flow instability is clearly of interest. It typically leads to turbulent flows; these may be important for dynamo action, through some mean-field α-effect, and also for the transport of mass and momentum, which can feed back on the large-scale flow.

Acknowledgements

This work was supported by the STFC doctoral training grant ST/F006934/1. We thank the referees for their useful comments. J.M. thanks E. Heifetz for helpful discussions.

Appendix A. Consistency checks for the long-wavelength jet analysis

The aim of this appendix is to show that

$$I = \frac{c^2 - M^2}{1 - F^2(c^2 - M^2)} \int_{-\infty}^{+\infty} \left(1 - \frac{c^2 - M^2}{(U - c)^2 - M^2}\right) \mathrm{d}y \tag{A 1}$$

is $O(\alpha \log \alpha)$, and hence that the asymptotic analysis of § 4.3.2 is consistent.

Following Drazin & Howard (1962), we assume that $|U| \leqslant A\mathrm{e}^{-a|y|}$, which is satisfied for the Bickley jet. They make the additional assumption that c is 'almost pure imaginary'; here we adopt the modified assumption that

$$\frac{|c|^2 + M^2}{c_i^2} \leqslant N = O(1), \tag{A 2}$$

which is supported by both our numerical and asymptotic results.

https://doi.org/10.1017/jfm.2015.718 Published online by Cambridge University Press

Consider first the case of $F = 0$ for which (A 1) is given by

$$I = (c^2 - M^2) \int_{-\infty}^{\infty} \left(1 - \frac{c^2 - M^2}{(U-c)^2 - M^2}\right) \mathrm{d}y. \tag{A 3}$$

For $y > 0$, we split the range of integration into $(0, \lambda)$ and (λ, ∞), where

$$\lambda = \log(A/c)^{1/a} = O(\log \alpha), \tag{A 4}$$

since $c^2 = O(\alpha)$. Then

$$\begin{aligned}(c^2 - M^2) \int_0^{\lambda} (\cdots)\,\mathrm{d}y &\leqslant |c^2 - M^2| \int_0^{\lambda} \left(1 + \frac{|c|^2 + M^2}{c_i^2}\right) \mathrm{d}y \\ &\leqslant |c^2 - M^2| \lambda (1 + N) = O(\alpha \log \alpha),\end{aligned} \tag{A 5}$$

where we have used the usual integral inequalities, the inequality $|(U-c)^2 - M^2| \geqslant c_i^2$, the assumption that $M^2 = O(\alpha)$ and the derived result (4.37) that $c = O(\alpha^{1/2})$.

Similarly,

$$\begin{aligned}(c^2 - M^2) \int_{\lambda}^{\infty} (\cdots)\,\mathrm{d}y &= (c^2 - M^2) \int_{\lambda}^{\infty} \left(\frac{U^2 - 2Uc}{(U-c)^2 - M^2}\right) \mathrm{d}y \\ &\leqslant \frac{|c^2 - M^2|}{c_i^2} \int_{\lambda}^{\infty} (U^2 + 2|U||c|)\,\mathrm{d}y \leqslant N \left(\frac{A^2 \mathrm{e}^{-2a\lambda}}{2a} + \frac{2A|c|\mathrm{e}^{-a\lambda}}{a}\right) \\ &= O(\alpha).\end{aligned} \tag{A 6}$$

The dominant contribution is from (A 5), and hence $I = O(\alpha \log \alpha)$.

When F is non-zero, the only difference is in the pre-factor to the integral (A 1). However, with c from either (4.37) or (4.38) the pre-factor is $O(1)$ and we may conclude that $I = O(\alpha \log \alpha)$.

Appendix B. Numerical method

We seek a numerical solution of the eigenvalue equation (2.7). Although the two velocity profiles considered are defined over the entire real line, we solve (2.7) on $y \in [-L, L]$. We employ a shooting method, which is numerically more efficient than solving the resulting linear algebra problem through a discretisation of the operators, particularly when the solution has small-scale features (see figure 12*c–e* for example). We shoot from the boundaries, with matching imposed at $y = 0$, employing a generalised Newton method as the root-finding algorithm. Since the solutions decay exponentially as $|y|$ becomes large, namely

$$G \sim \exp(-\alpha K_{\pm} y) \quad \text{as } |y| \to \infty, \tag{B 1}$$

where

$$K_{\pm}^2 = 1 - F^2((U_{\pm} - c)^2 - M^2), \quad U_{\pm} = \lim_{y \to \pm\infty} U(y), \tag{B 2a,b}$$

we adopt expression (B 1) as the boundary condition to be implemented at $y = \pm L$. Since our interest is in instabilities, singularities in the governing equation are avoided. To ensure negligible influence of the finite domain, L is doubled until the computed eigenvalue changes by less than 0.5 %. The routines are written in MATLAB, using

https://doi.org/10.1017/jfm.2015.718 Published online by Cambridge University Press

`ode113` as the integrator (an Adams–Bashforth method with adaptive grid). Although the boundary conditions are functions of c, changing at every iteration, we generally have no problems with convergence provided that the initial guess is close to the true value. Solutions are initialised from $(M, F) = (0, 0)$ at some fixed α using a known numerical result documented in, for example, Drazin & Reid (1981). Runs at new parameter values are then initialised using a linear extrapolation for c from previously calculated values at nearby parameters.

REFERENCES

Balmforth, N. J. 1999 Shear instability in shallow water. *J. Fluid Mech.* **387**, 97–127.

Bazdenkov, S. V. & Pogutse, O. P. 1983 Supersonic stabilization of a tangential shear in a thin atmosphere. *J. Expl Theor. Phys. Lett.* **37**, 375–377.

Blumen, W., Drazin, P. G. & Billings, D. F. 1975 Shear layer instability of an inviscid compressible fluid. Part 2. *J. Fluid Mech.* **71**, 305–316.

Bretherton, F. P. 1966 Baroclinic instability and the short wavelength cut-off in terms of potential vorticity. *Q. J. R. Meteorol. Soc.* **92**, 335–345.

Cally, P. S. 2003 Three-dimensional magneto-shear instabilities in the solar tachocline. *Mon. Not. R. Astron. Soc.* **339**, 957–972.

Carpenter, J. R., Tedford, E. W., Heifetz, E. & Lawrence, G. A. 2012 Instability in stratified shear flow: review of a physical interpretation based on interacting waves. *Appl. Mech. Rev.* **64**, 061001.

Caulfield, C. P. 1994 Multiple linear instability of layered stratified shear flow. *J. Fluid Mech.* **258**, 255–285.

Chen, X. L. & Morrison, P. J. 1991 A sufficient condition for the ideal instability of shear flow with parallel magnetic field. *Phys. Fluids* B **3**, 863–865.

Collings, I. L. & Grimshaw, R. H. J. 1980 The effect of topography on the stability of a barotropic coastal current. *Dyn. Atmos. Oceans* **5**, 83–106.

De Sterck, H. 2001 Hyperbolic theory of the 'shallow water' magnetohydrodynamics equations. *Phys. Plasmas* **8**, 3293–3304.

Dellar, P. J. 2002 Hamiltonian and symmetric hyperbolic structures of shallow water magnetohydrodynamics. *Phys. Plasmas* **9**, 1130–1136.

Dikpati, M. & Gilman, P. A. 2001 Analysis of hydrodynamic stability of solar tachocline latitudinal differential rotation using a shallow-water model. *Astrophys. J.* **551**, 536–564.

Dikpati, M., Gilman, P. A. & Rempel, M. 2003 Stability analysis of tachocline latitudinal differential rotation and coexisting toroidal band using a shallow-water model. *Astrophys. J.* **596**, 680–697.

Drazin, P. G. & Howard, L. N. 1962 The instability to long waves of unbounded parallel inviscid flow. *J. Fluid Mech.* **14**, 257–283.

Drazin, P. G. & Howard, L. N. 1966 Hydrodynamic stability of parallel flow of inviscid fluid. *Adv. Appl. Mech.* **9**, 1–89.

Drazin, P. G. & Reid, W. H. 1981 *Hydrodynamic Stability*, 2nd edn. Cambridge University Press.

Gedzelman, S. D. 1973 Hydromagnetic stability of parallel flow of an ideal heterogeneous fluid. *J. Fluid Mech.* **58**, 777–794.

Gill, A. E. 1965 Instabilities of 'top-hat' jets and wakes in compressible fluids. *Phys. Fluids* **8**, 1428–1430.

Gill, A. E. 1982 *Atmosphere-Ocean Dynamics*. Academic.

Gill, A. E. & Drazin, P. G. 1965 Note on instability of compressible jets and wakes to long-wave disturbances. *J. Fluid Mech.* **22**, 415.

Gilman, P. A. 1967 Stability of baroclinic flows in a zonal magnetic field: part I. *J. Atmos. Sci.* **24**, 101–118.

https://doi.org/10.1017/jfm.2015.718 Published online by Cambridge University Press

GILMAN, P. A. 2000 Magnetohydrodynamic 'shallow water' equations for the solar tachocline. *Astrophys. J.* **544**, L79–L82.

GILMAN, P. A. & CALLY, P. S. 2007 Global MHD instabilities of the tachocline. In *The Solar Tachocline* (ed. D. W. Hughes, R. Rosner & N. O. Weiss), Cambridge University Press.

GILMAN, P. A. & DIKPATI, M. 2002 Analysis of instability of latitudinal differential rotation and toroidal field in the solar tachocline using a magnetohydrodynamic shallow-water model. I. Instability for broad toroidal field profiles. *Astrophys. J.* **576**, 1031–1047.

GOUGH, D. O. 2007 An introduction to the solar tachocline. In *The Solar Tachocline* (ed. D. W. Hughes, R. Rosner & N. O. Weiss), Cambridge University Press.

HARNIK, N. & HEIFETZ, E. 2007 Relating overreflection and wave geometry to the counter-propagating Rossby wave perspective: toward a deeper mechanistic understanding of shear instability. *J. Atmos. Sci.* **64**, 2238–2261.

HAYASHI, Y.-Y. & YOUNG, W. R. 1987 Stable and unstable shear modes of rotating parallel flows in shallow water. *J. Fluid Mech.* **184**, 477–504.

HEIFETZ, E., MAK, J., NYCANDER, J. & UMURHAN, O. M. 2015 Interacting vorticity waves as an instability mechanism for magnetohydrodynamic shear instabilities. *J. Fluid Mech.* **767**, 199–225.

HENG, K. & SPITKOVSKY, A. 2009 Magnetohydrodynamic shallow water waves: linear analysis. *Astrophys. J.* **703**, 1819–1831.

HØILAND, E. 1953 On two-dimensional perturbation of linear flow. *Geophys. Publ.* **18**, 333–342.

HOSKINS, B. J., MCINTYRE, M. E. & ROBERTSON, A. W. 1985 On the use and significance of isentropic potential vorticity maps. *Q. J. R. Meteorol. Soc.* **111**, 877–946.

HOWARD, L. N. 1961 Note on a paper of John W. Miles. *J. Fluid Mech.* **10**, 509–512.

HOWARD, L. N. 1963 Neutral curves and stability boundaries in stratified flow. *J. Fluid Mech.* **16**, 333–342.

HUGHES, D. W., ROSNER, R. & WEISS, N. O. 2007 *The Solar Tachocline*. Cambridge University Press.

HUGHES, D. W. & TOBIAS, S. M. 2001 On the instability of magnetohydrodynamic shear flows. *Proc. R. Soc. Lond.* A **457**, 1365–1384.

LIPPS, F. B. 1962 The barotropic stability of the mean winds in the atmosphere. *J. Fluid Mech.* **12**, 397–407.

MAK, J. 2013 Shear instabilities in shallow-water magnetohydrodynamics. PhD thesis, University of Leeds.

MICHAEL, D. H. 1955 Stability of a combined current and vortex sheet in a perfectly conducting fluid. *Proc. Camb. Phil. Soc.* **51**, 528–532.

MICHALKE, A. 1964 On the inviscid instability of the hyperbolic-tangent velocity profile. *J. Fluid Mech.* **19**, 543–556.

MILES, J. W. 1958 On the disturbed motion of a vortex sheet. *J. Fluid Mech.* **4**, 538–552.

MIURA, A. & PRITCHETT, P. L. 1982 Nonlocal stability analysis of the MHD Kelvin–Helmholtz instability in a compressible plasma. *J. Geophys. Res.* **87**, 7431–7444.

PEDLOSKY, J. 1964 The stability of currents in the atmosphere and the ocean: part I. *J. Atmos. Sci.* **21**, 201–219.

RABINOVICH, A., UMURHAN, O. M., HARNIK, N., LOTT, F. & HEIFETZ, E. 2011 Vorticity inversion and action-at-a-distance instability in stably stratified shear flow. *J. Fluid Mech.* **670**, 301–325.

RAYLEIGH, L. 1878 On the instability of jets. *Proc. Lond. Math. Soc.* **10**, 4–12.

RIPA, P. 1983 General stability conditions for zonal flows in a one-layer model on the β-plane or the sphere. *J. Fluid Mech.* **126**, 463–489.

SATOMURA, T. 1981 An investigation of shear instability in a shallow water. *J. Met. Soc. Japan* **59**, 148–170.

SCHECTER, D. A., BOYD, J. F. & GILMAN, P. A. 2001 'Shallow-water' magnetohydrodynamic waves in the solar tachocline. *Astrophys. J.* **551**, L185–L188.

SHIVAMOGGI, B. K. & DEBNATH, L. 1987 Stability of magnetohydrodynamic stratified shear flows. *Acta Mechanica* **68**, 33–42.

https://doi.org/10.1017/jfm.2015.718 Published online by Cambridge University Press

STERN, M. E. 1963 Joint instability of hydromagnetic fields which are separately stable. *Phys. Fluids* **6**, 636–642.

SUTHERLAND, B. R. & PELTIER, W. R. 1992 The stability of stratified jets. *Geophys. Astrophys. Fluid Dyn.* **66**, 101–131.

TAKEHIRO, S. I. & HAYASHI, Y. Y. 1992 Over-reflection and shear instability in a shallow-water model. *J. Fluid Mech.* **236**, 259–279.

VALLIS, G. K. 2006 *Atmospheric and Oceanic Fluid Dynamics*. Cambridge University Press.

ZAQARASHVILI, T. V., OLIVER, R., BALLESTER, J. L. & SHERGELASHVILI, B. M. 2007 Rossby waves in 'shallow water' magnetohydrodynamics. *Astron. Astrophys.* **470**, 815–820.

https://doi.org/10.1017/jfm.2015.718 Published online by Cambridge University Press